BLUE/GREEN COUPLED WAVE FILTER DEMONSTRATION

J. F. Lotspeich and D. M. Henderson

Hughes Research Laboratories
3011 Malibu Canyon Road
Malibu, CA 90265

May 1981

Contract No. N00014-80-C-0606

Final Report

For period 4 June 1980 through 28 February 1981

Approved for public release; distribution unlimited.

Sponsored By
OFFICE OF NAVAL RESEARCH
Physical Sciences Division
Arlington, Virginia 22217

UNCLASSIFIED

SECURITY CLASSIFICATION OF THIS PAGE (When Data Entered)

REPORT DOCUMENTATION PAGE	READ INSTRUCTIONS BEFORE COMPLETING FORM
1. REPORT NUMBER	2. GOVT ACCESSION NO. AD-A099159	3. RECIPIENT'S CATALOG NUMBER
4. TITLE (and Subtitle) BLUE/GREEN COUPLED WAVE FILTER DEMONSTRATION	5. TYPE OF REPORT & PERIOD COVERED Final Report, 4 Jun 1980-28 Feb 1981
	6. PERFORMING ORG. REPORT NUMBER
7. AUTHOR(s) J.F. Lotspeich and D.M. Henderson	8. CONTRACT OR GRANT NUMBER(s) N00014-80-C-0606
9. PERFORMING ORGANIZATION NAME AND ADDRESS Hughes Research Laboratories 3011 Malibu Canyon Road Malibu, California 90265	10. PROGRAM ELEMENT, PROJECT, TASK AREA & WORK UNIT NUMBERS Project 421
11. CONTROLLING OFFICE NAME AND ADDRESS Office of Naval Research Physical Sciences Division Arlington, Virginia 22217	12. REPORT DATE May 1981
	13. NUMBER OF PAGES 61
14. MONITORING AGENCY NAME & ADDRESS(if different from Controlling Office)	15. SECURITY CLASS (of this report) UNCLASSIFIED
	15a. DECLASSIFICATION DOWNGRADING SCHEDULE

16. DISTRIBUTION STATEMENT (of this Report)

Approved for public release; distribution unlimited.

17. DISTRIBUTION STATEMENT (of the abstract entered in Block 20, if different from Report)

18. SUPPLEMENTARY NOTES

19. KEY WORDS (Continue on reverse side if necessary and identify by block number)

Optical filter
Blue-green band
Iso index characteristic
Electro-optic coupling
Optical activity
Computer simulation

20. ABSTRACT (Continue on reverse side if necessary and identify by block number)

The performance of $AgGaS_2$ iso-index coupled-wave electro-optic filters in wide-field of view (FOV) operation has been characterized in detail, both theoretically and experimentally. The principal conclusions of this program are: (1) The effect of optical activity on the filter passband is negligible for input light cones smaller than approx. f/10 (3° half-angle). (2) For larger FOVs, the main lobe of the filter transfer

Cont'd

DD FORM 1 JAN 73 1473 EDITION OF 1 NOV 65 IS OBSOLETE

UNCLASSIFIED

SECURITY CLASSIFICATION OF THIS PAGE (When Data Entered)

1726 cc

characteristic broadens considerably, and increased out-of-band transmission occurs. (3) At very large FOVs (approx. f/0.5), the peak transmittance approaches 50%, virtually independent of applied electric field. (4) The effects of optical activity override attempts to narrow the passband by increasing filter length, resulting in an optimum crystal length of about 3 mm and a minimum passband of about 2 Å for f/1 FOV (1 Å for f/2 FOV). (5) Significant reduction in out-of-band transmission was shown, using a novel dual-element arrangement with intervening crossed polarizer.

FOREWORD

This is the final technical report on Contract N00014-80-C-0606, Project 421. The work reported here was accomplished by Hughes Research Laboratories, a division of Hughes Aircraft Company, 3011 Malibu Canyon Road, Malibu, CA 90265. This research was accomplished during the period 4 June 1980 through 23 February 1981. The U.S. Navy program monitor was M.B. White, Code 421. This document was submitted on 14 May 1981; its authors were J.F. Lotspeich, principal investigator, and D.M. Henderson, program manager.

The coupled-mode analysis of optical activity in uniaxial electro-optic crystals is the original contribution of Prof. Amnon Yariv of the California Institute of Technology, and is gratefully acknowledged.

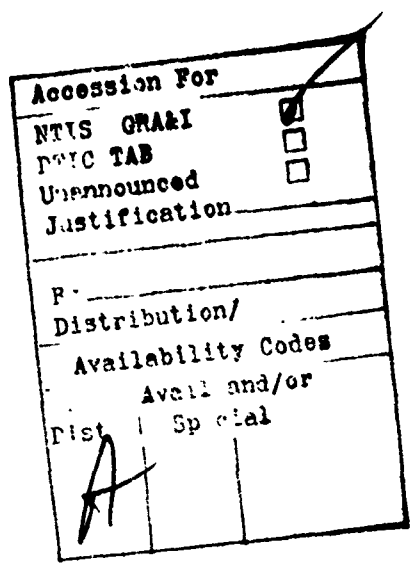

TABLE OF CONTENTS

LIST OF ILLUSTRATIONS

SECTION 1

INTRODUCTION AND SUMMARY

The ability of light in the blue-green portion of the spectrum to penetrate operational-depth sea water has created increased interest in optical communications from space and airborne platforms directly to submerged terminals. Of the various blue/green optical communications programs, the most demanding requirements are set by strategic laser communications (SLC), in which information is transmitted from a synchronous satellite or relay mirror to a submarine at depth. The link requires a filter with a bandwidth of ∿0.1 Å and field of view (FOV) of ±45° (∿f/0.5 optics). These requirements cannot be simultaneously met with conventional filters (such as dielectric layer interference filters).

Although optical communications to submerged stations has been of considerable interest to the Navy since the invention of the laser, projected systems performance has been severely limited by the available receiver technology. Several factors complicate the problem in a marine environment, including loss of coherence caused by multiple scattering, wavefront distortion in passing through the air-water interface and uncertainty in target location that requires the target to be greatly over-illuminated.

The blue-green filters require a wide FOV to allow the transmitted laser light, scattered by the air-sea interface, and the sea water itself, to be efficiently collected. The filter must also have a very narrow passband to minimize the background sunlight and bioluminescence. In conventional interference filter approaches, the two requirements are contradictory. Conventional interference filters include Fabry-Perot, dielectric layer interference, acousto-optic, and birefringent (Lyot and Solc) filters.

Since conventional filter techniques cannot meet the blue-green requirements, new approaches are needed. A modified Lyot filter developed by Lockheed, with a bandwidth of ∿1 Å, FOV of ±30°, and peak transmission of ∿40%, is projected to be the state of the art in blue/green filters. Narrowband atomic resonance filters, investigated by Lawrence Livermore Laboratory and McDonnell-Douglas, exhibit promising features but operate at a fixed wavelength and have a limited efficiency. An interesting variation of the

Lyot filter has recently been proposed by workers at Rockwell in which crystals having a highly dispersive birefringence, such as CdS, are used. The resultant enhancement in the wavelength dependence of relative phase retardation allows for a large reduction in overall length of the filter, with a concommitant large increase in FOV.

The present work at Hughes has followed two earlier Navy contracts in 1978 (N00014-78-C-0201) and 1979 (N00014-79-C-0491). In 1978 we undertook the investigation of new filter approaches to meet the challenging requirements of satellite-to-submarine communications. That study led to the concept of the iso-index coupled-wave filter in which polarized light is selectively coupled from the fast to the slow axes in certain birefringent crystals exhibiting a zero crossing in their birefringence. This zero-crossing point is referred to as the iso-index point. The calculated performance of this class of filters showed great promise for meeting blue/green requirements. For example, a filter of $AgGaS_2$ which has its iso-index point at 4970 Å showed a calculated bandwidth of $\sim$0.2 Å over a full 2π sr FOV.

In the 1979 program, we fabricated test devices and demonstrated the narrow-bandwidth properties offered by this technique. Specifically, our $AgGaS_2$ filters with 3 mm interaction length showed a 0.94-Å bandwidth. This translated to a bandwidth of 0.3 Å in a 1 cm sample. Preliminary measurements also showed that the bandwidth degraded insignificantly with extreme off-axis light, as expected from our initial theoretical calculations. The largest offset measured was $\pm 60°$, which corresponds to an f/0.3 optical system. Temperature tuning of the filter above 4970 Å was demonstrated with a measured tuning rate of $\sim$0.25 Å/°C.

However, during the course of the present program, we determined that it is not possible to extend the performance of the $AgGaS_2$ iso-index filter down to the 0.3-Å bandwidth because of the effects of optical activity present in the tetragonal ($\bar{4}2m$) crystals like $AgGaS_2$. For this reason, we redirected our efforts away from the original plan of fabricating high-quality, large-area ($\sim$1 cm^2) filter elements to a concentrated study effort aimed at a complete analytical characterization of the $AgGaS_2$ capabilities and limitations, together with supporting experimental data.

Principal conclusions of this program are: (1) The effect of optical activity on the $AgGaS_2$ iso-index filter passband is negligible for input light cones smaller than ∿f/10 (3° half-angle). (2) For larger FOVs, the main lobe of the filter transfer characteristic broadens considerably, and increased out-of-band transmission occurs. (3) At very large FOV (∿f/0.5) the peak transmittance approaches 50%, virtually independent of the applied electric field. (4) The effects of optical activity override attempts to narrow the passband by increasing filter length, resulting in an optimum crystal length of about 3 mm and a minimum passband of about 2 Å for f/1 FOV (1 Å for f/2 FOV). (5) Significant reduction in out-of-band transmission was shown to result using a novel dual-element arrangement with intervening crossed polarizer. Most effective suppression occurred with elements of unequal length, so chosen that the first few sidelobes of one element peaked at or near the zeroes of the other element.

In Section 2 we briefly review the operating principles of the iso-index filter. Section 3 describes relevant optical and electro-optic characteristics of $AgGaS_2$, including optical activity and its consequences. In Section 4 we discuss computer modeling of the $AgGaS_2$ filter and show comparisons with experimental results. Section 5 extends the modeling predictions to wide-FOV operation. Conclusions and recommendations are presented in Section 6.

SECTION 2

TECHNICAL BACKGROUND

During our 1978 exploratory contract study of novel techniques for narrowband, wide-FOV filtering in the blue/green spectral band, a promising new kind of optical filter was designed.[1,2,3] This device is based on the zero crossing of birefringence that occurs near the band edge in certain uniaxial crystals, one noteworthy example being $AgGaS_2$. Coupling of light energy is induced between principal polarizations at the isotropic point by a dc electric field. When placed between crossed polarizers, the crystals may thus act as narrow-band filters. The device is called, accordingly, an iso-index coupled-wave electro-optic filter. The unique features of this and related filters[4,5] are their simultaneous high selectivity and very wide FOV.

The filter configuration is illustrated in Figure 1, together with the wavelength-dependent birefringence of $AgGaS_2$, and the resultant theoretical filter transfer characteristic for a 1 cm sample. An alternative selection of crystal cut allows the use of a transverse, rather than longitudinal, electric field, as shown in Figure 2(b). The transfer characteristic shown in Figure 1 is an idealized representation that neglects the effects of optical activity present in $AgGaS_2$. This is elaborated in Section 3. Applying an electric field $\mathscr{E}_1$ in a direction normal to the optic axis in a crystal such as $AgGaS_2$ ($\bar{4}2m$ symmetry) causes the optic axis to rotate through an angle α according to

$$\tan 2\alpha = \frac{2n_o^2 n_e^2 r_{41} \mathscr{E}_1}{n_o^2 - n_e^2} \quad , \tag{1}$$

where n_o and n_e are the ordinary and extraordinary refractive indices, respectively, and r_{41} is the relevant electro-optic tensor component. With finite birefringence, α is in practice a very small angle. Thus, light entering the crystal and having its polarization either parallel or perpendicular to the original optic axis will essentially maintain that direction through the crystal and be blocked by a crossed analyzer. At a particular wavelength λ_o where the birefringence disappears (in zero field),

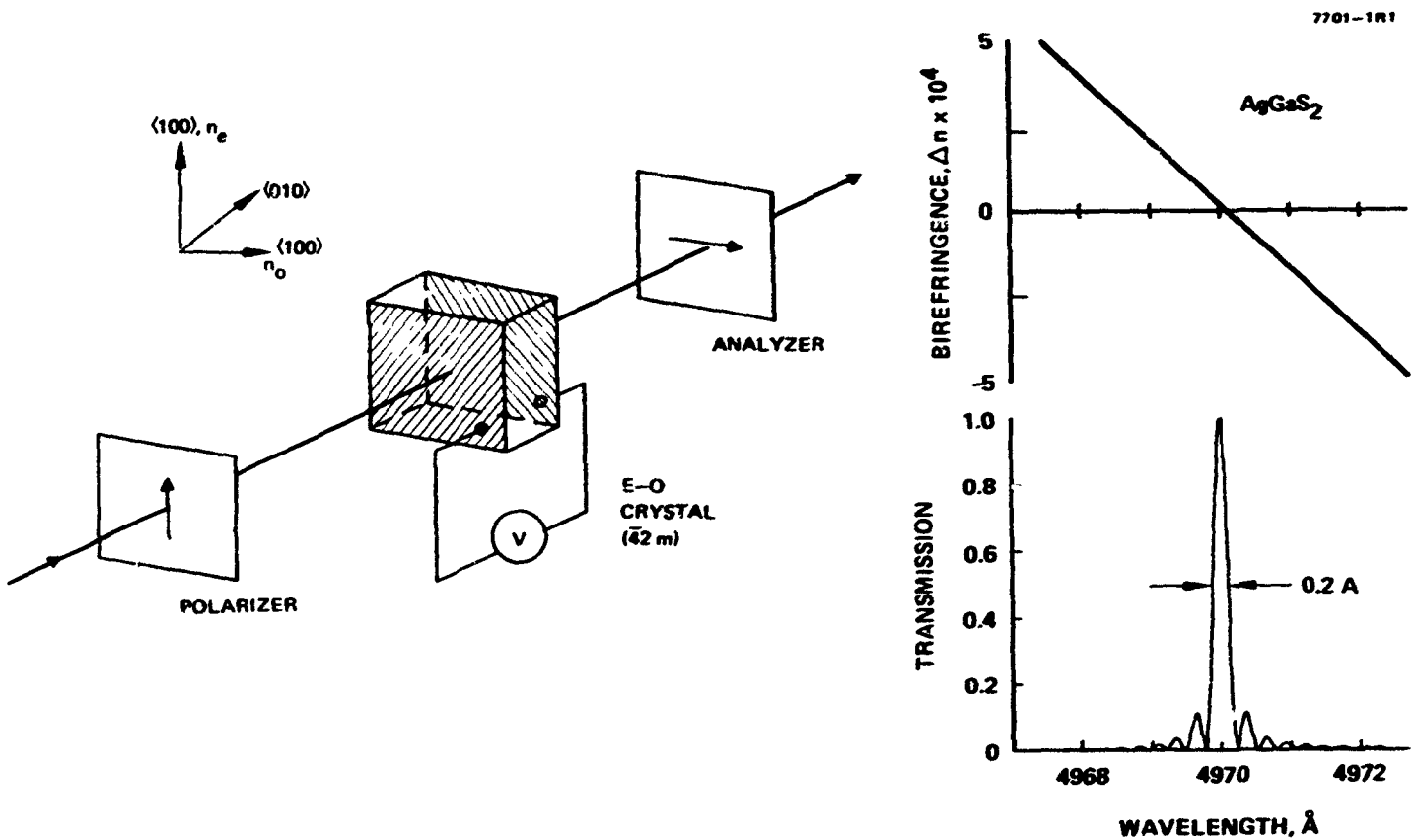

Figure 1. Iso-index coupled-wave electro-optic filter configuration, showing wavelength-dependent birefringence of $AgGaS_2$ and resultant filter transfer characteristic for a 1-cm sample, with half-wave voltage applied. This is an idealized representation that neglects the effects of optical activity. See later text.

7701 1

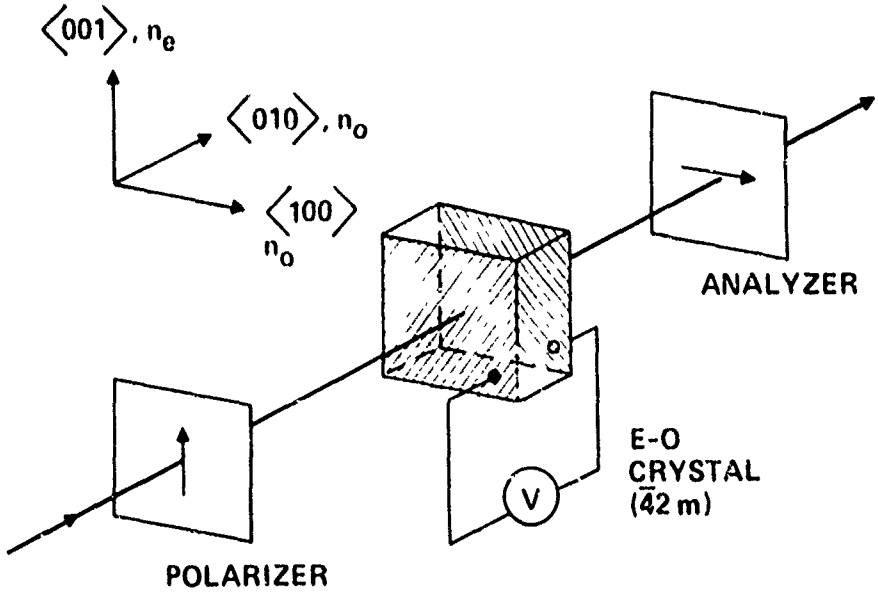

(a) Longitudinal field

7701-2

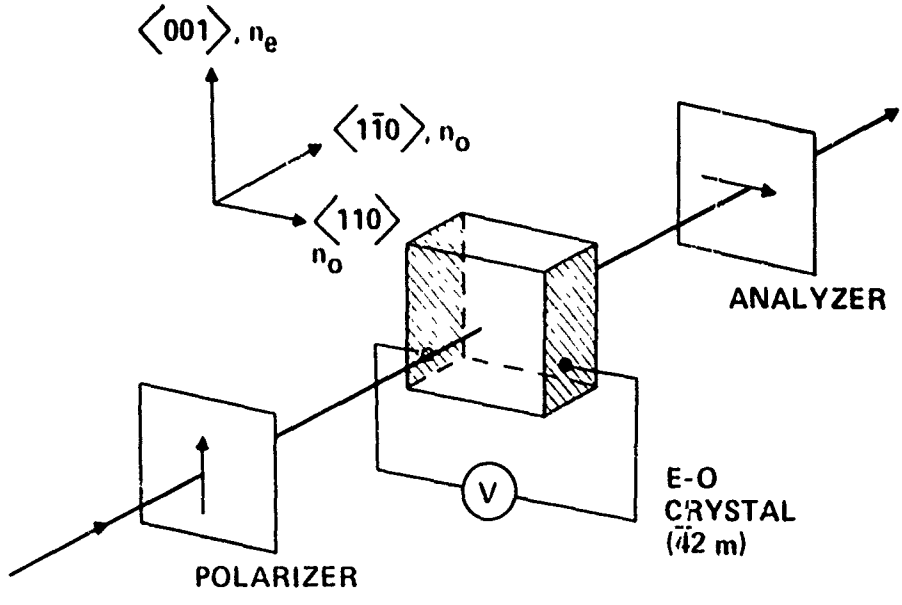

(b) Transverse field

Figure 2. Coupled-wave electro-optic filter configurations.

α goes abruptly to 45°, according to Eq. 1, and the field-induced changes in the values of the refractive indices depend on $\mathscr{E}_1$ as

$$n_e \rightarrow \bar{n} + \frac{1}{2}\bar{n}^3 r_{41}\mathscr{E}_1$$

$$n_o \rightarrow \bar{n} - \frac{1}{2}\bar{n}^3 r_{41}\mathscr{E}_1 \quad , \tag{2}$$

where $\bar{n}$ is the average (common) value of n_e and n_o. For this condition, the crystal now has the configuration of a classic Pockels cell.

The transfer characteristic τ of a lossless filter of length L as a function of wavelength is given by coupled-mode theory:[4]

$$\tau = \frac{(\Gamma L)^2 \sin^2 \sqrt{(\Gamma L)^2 + (\Delta kL/2)^2}}{(\Gamma L)^2 + (\Delta kL/2)^2} \quad , \tag{3}$$

where

$$\Gamma = \frac{\pi}{\lambda}\bar{n}^3 r_{41}\mathscr{E}_1 \quad , \tag{4}$$

and

$$\Delta k = \frac{2\pi}{\lambda}(n_e - n_o) \quad . \tag{5}$$

An important feature of this type of filter is its selectivity. This is determined by the rate at which the birefringence, $n_e - n_o$, passes through zero. For example, $AgGaS_2$ exhibits a birefringence[6] with a very abrupt passage thrcugh zero at 4970 Å. A crystal having a total interaction length of 1 cm would theoretically have a 3 dB passband of only 0.2 Å, in the absence of optical activity, and would give full transmission with an applied voltage of a few kilovolts.

An equally important co-feature is the wide FOV characteristic. Theory indicates a limiting FOV of 2π sr with less than a 20% increase in passband

over the narrow-field case. The physical reason for the wide FOV is that optical phase matching occurs at all angles at the resonant wavelength.

We emphasize that the above principles and specifications are valid only for crystals that exhibit very little or no optical activity. The effect of optical activity may be characterized in general as an angle-dependent coupling of polarization components in the absence of other external stimuli. A generalized coupled-mode theory for iso-index electro-optic crystals where optical activity is present is given in the Appendices.

SECTION 3

PROPERTIES OF $AgGaS_2$

A. BIREFRINGENCE AND ISO-INDEX POINT

The behavior of the two indices of refraction of $AgGaS_2$ in the visible range of wavelengths is shown in Figure 3. These data were taken from Reference 6. Note the zero crossing of the birefringence at 497 nm. This is the point of operation of the iso-index coupled-wave electro-optic filter. The rapid rate of change of birefringence with wavelength through the iso-index point determines the high degree of selectivity of this kind of filter.

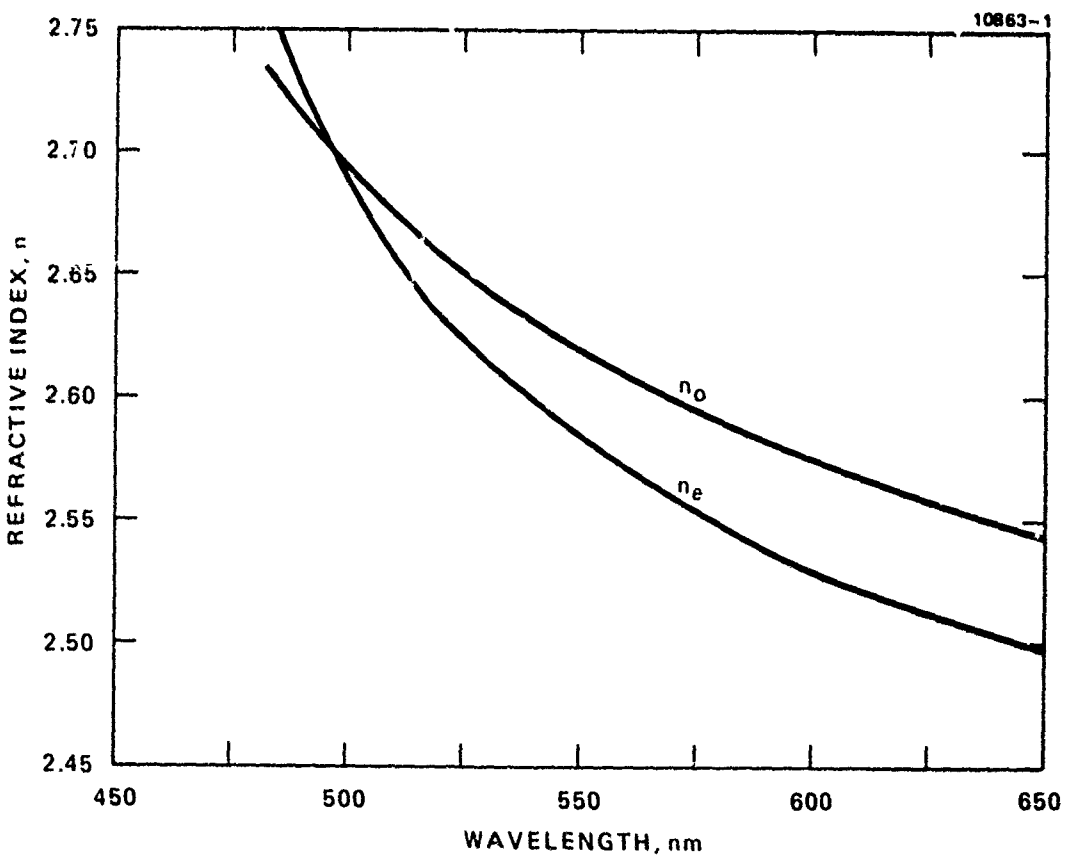

Figure 3. Dispersion curves of $AgGaS_2$ showing the zero crossing of birefringence at 497 nm. (Data of Reference 6.)

B. ELECTRO-OPTIC AND ELASTO-OPTIC EFFECT

Coupling of light energy between principal polarizations can be induced in $AgGaS_2$ at the iso-index point by application of a properly oriented electric field or elastic strain. By virtue of the tetragonal ($\bar{4}2m$) symmetry of $AgGaS_2$, there are only three non-zero electro-optic tensor components: $r_{41} = r_{52}$, and r_{63}. Either r_{41} or r_{52}, in conjunction with electric fields applied in the x-y plane, are instrumental in activating the refractive perturbations in $AgGaS_2$ that give rise to the light coupling, as described in Section 2. By symmetry, many of the elasto-optic tensor components of $AgGaS_2$ are also zero; and of the remaining non-zero members, a number are equal. The non-zero components are: $p_{11} = p_{22}$, $p_{12} = p_{21}$, $p_{13} = p_{23}$, $p_{31} = p_{32}$, p_{33}, $p_{44} = p_{55}$, and p_{66}. The relevant components for elasto-optic stimulus of the iso-index filter are p_{44} or p_{55}, associated with shear strains in the y-z and x-z planes, respectively; both engender a rocking of the optic axis in those same corresponding planes. It is a simple exercise in tensor transformation to show that a shear strain in any plane containing the optic axis is equivalent to a shear strain in the x-z plane, and that the optic axis rocking always occurs in the plane of shear. The magnitude of this perturbation is given by Eq. 1 in which $r_{41}\mathcal{E}_1$ is replaced by $p_{44}S_4$ (or $p_{55}S_5$), S being the shear strain.

C. OPTICAL ACTIVITY

In crystals exhibiting pure optical activity, plane-polarized light suffers a rotation of the plane of polarization when passing along certain directions through the crystal. The magnitude of this rotation is directly proportional to the distance traversed. This phenomenon is explained by showing that the eigenmodes of polarization are right and left circular, instead of linear or plane, as is the case for pure linear birefringence. Polarization rotation results from a differential phase retardation of the circular modes into which the plane-polarized wave is decomposed, as shown by the top illustration of Figure 4. The phasors A and B represent the right and left circular modes into which the initial vertically-polarized beam C is

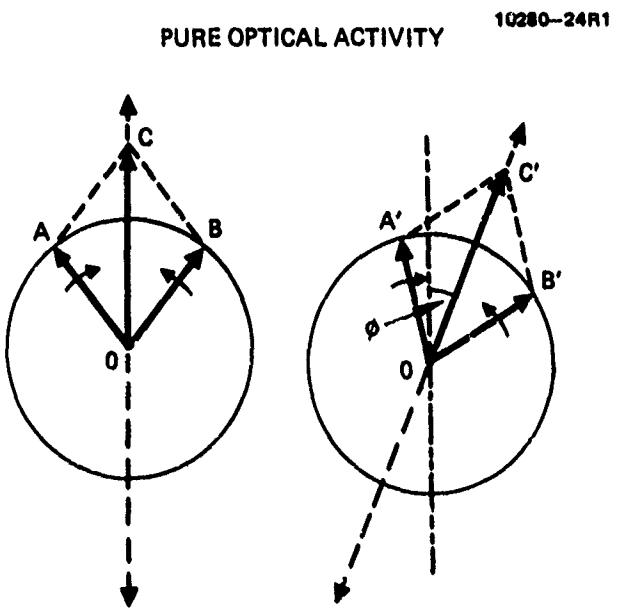

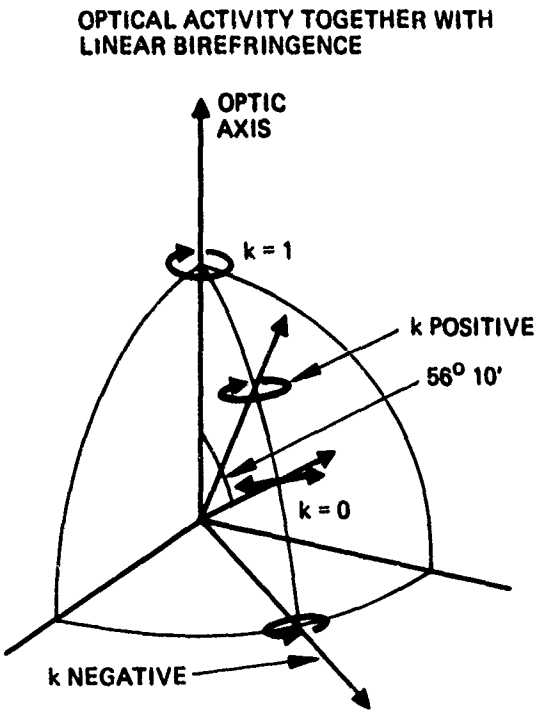

Figure 4. Illustrating optical activity with and without concurrent linear birefringence. The lower illustration represents the ordinary ray in quartz. (Taken from Reference 7.)

decomposed. The primed phasors show the relative positions at the output of the crystal, and the resultant rotated plane of polarization, C'.

When linear and circular birefringence exist concurrently in a crystal, as is the case with $AgGaS_2$, the eigenmodes are, in general, elliptically polarized. Since the circular birefringence varies tensorially with direction through the crystal, certain directions will show pure circular birefringence, while other directions will show only linear birefringence. Thus, the ellipticity will vary from ±1 to 0. This is illustrated in the lower half of Figure 4, which shows the evolution of ellipticity (denoted by k) of an ordinary ray in quartz as the light propagation direction varies angularly from the x-y plane to the optic axis. A detailed discussion of these phenomena, as well as the symmetry properties of the gyration tensor for the various crystal classes, is given in Reference 7, from which Figure 4 was adapted.

The maximum optical rotatory power in $AgGaS_2$ occurs along the <100> and <010> directions, and has a strength[8] of ±522 deg/mm at the iso-index point, 497 nm.

D. CONSEQUENCES OF OPTICAL ACTIVITY IN $AgGaS_2$ FOR ISO-INDEX FILTER APPLICATIONS

In Sections 4 and 5 we will discuss in detail computer-modeled transfer characteristics, and supporting experimental data, for $AgGaS_2$ filter samples that illustrate the limitations to selectivity imposed by optical activity when wide FOVs are involved. In summary, we will mention the salient features involved.

So long as we restrict outselves to an essentially one-dimensional FOV with ray propagation anywhere in the (110) or $(1\bar{1}0)$ plane, ideal filter performance, as shown in Figure 1, may be achieved because optical activity is null for those directions of propagation. For practical two-dimensional FOVs, however, coupling of polarizations occurs — with or without applied electric field — at wavelengths well outside the limits otherwise dictated by the ideal filter passband of Figure 1. The net result is that passbands are broadened considerably at large FOV (∿f/1 to f/0.5), out-of-band transmission is significantly increased, and maximum attainable peak transmittances approach 50% (for polarized light), essentially independent of applied voltage.

Many other crystal classes besides that of $AgGaS_2$ ($\bar{4}2m$) can exhibit optical activity, based on symmetry considerations.[7] For completeness we show in Figure 5 all of the possible symmetry choices available for iso-index filter applications. Of course, not all crystal candidates exhibit the zero crossing of birefringence; but those indicated in Figure 5 are candidates at least in principle. It is seen from Figure 5 that optical activity is the rule rather than the exception: only hexagonal class 6mm, trigonal class 3m, and tetragonal class 4mm are free of optical activity; and these are all types that are applicable exclusively to transverse electric field filters.

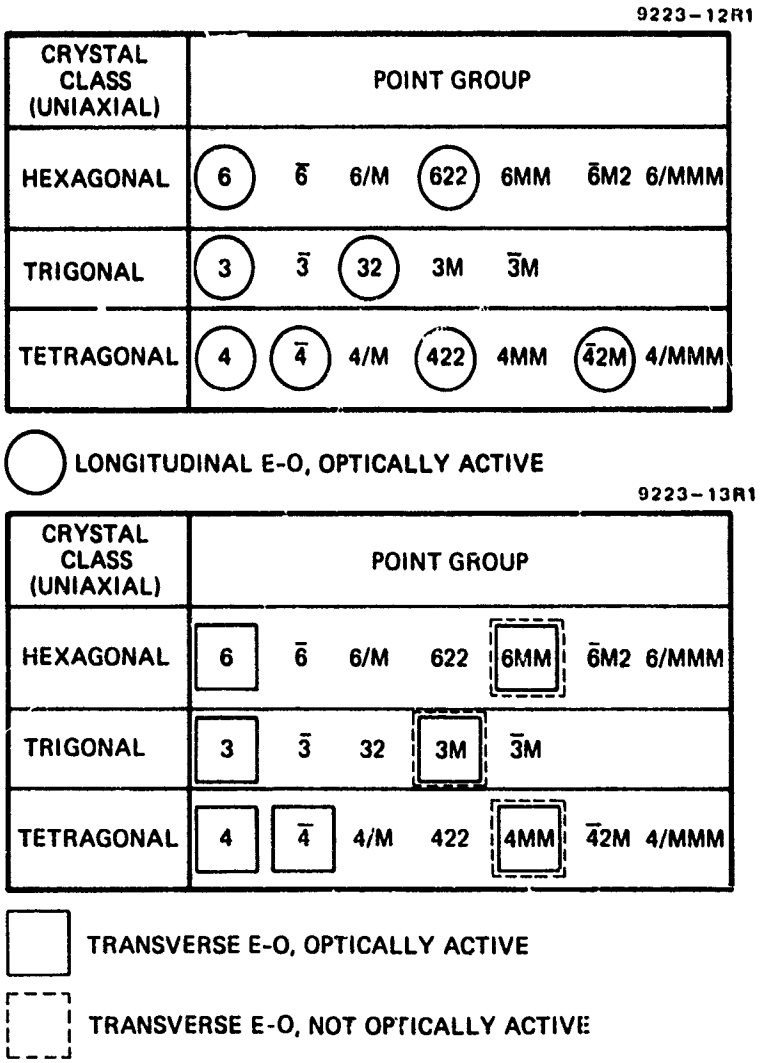

Figure 5. Point groups pertinent to iso-index filters, showing optically- and non-optically-active classes.

SECTION 4

COMPUTER MODELING AND EXPERIMENTAL VERIFICATION

A. THEORY INCLUDING OPTICAL ACTIVITY

In describing the coupling of light energy from one principal polarization to another, it is convenient to use the matrix operator formalism,

$$\vec{E}(L) = \mathbf{G} \cdot \vec{E}(0) \quad , \tag{6}$$

where $\vec{E}$ is the electric field of the light wave, assumed to be propagating in a direction y through the cyrstal, and where $\mathbf{G}$ is an operator that transforms the field at y = 0 to a new field at y = L. In a 2-dimensional matrix notation,

$$\vec{E}(y) = \begin{pmatrix} X(y) \\ Z(y) \end{pmatrix} e^{-j\bar{k}y} \quad , \tag{7}$$

and

$$\mathbf{G} = \mathbf{G}(y) = \begin{pmatrix} G_{11} & G_{12} \\ G_{21} & G_{22} \end{pmatrix} \quad , \tag{8}$$

where $\bar{k} = 1/2(k_x + k_z)$ is the average of the eigenmode propagation constants, k_x and k_z, belonging to a base representation of linearly-polarized eigenmodes.

From the generalized coupled-mode theory developed in Appendix A, we can show that the explicit expressions for the polarization component amplitudes are

$$X(y) = \left(\frac{\kappa + j\Gamma}{s}\right) Z(0)\sin sy + X(0)\left[\cos sy + j\left(\frac{\delta}{s}\right)\sin sy\right] \quad , \tag{9}$$

and

$$Z(y) = \left(\frac{-\kappa + j\Gamma}{s}\right) X(0)\sin sy + Z(0)\left[\cos sy - j\left(\frac{\delta}{s}\right)\sin sy\right] \quad , \tag{10}$$

in which κ is the specific rotation (in the absence of birefringence), Γ is the electro-optic coupling coefficient or specific phase retardation,

(see Eq. 4), and δ is a birefringence parameter (see Eq. 5),

$$\delta = \frac{1}{2}(k_z - k_x) = \frac{1}{2}\Delta k \quad . \tag{11}$$

The symbol s represents the "vectorial sum" of κ, Γ, and δ:

$$s = (\kappa^2 + \Gamma^2 + \delta^2)^{1/2} \quad . \tag{12}$$

By inspection of Eqs. 9 and 10 we can immediately write down the expressions for the matrix elements of the **G** operator:

$$G_{11} = \text{cossy} + j\left(\frac{\delta}{s}\right)\text{sinsy} \quad , \tag{13}$$

$$G_{12} = \left(\frac{\kappa + j\Gamma}{s}\right)\text{sinsy} \quad , \tag{14}$$

$$G_{21} = \left(\frac{-\kappa + j\Gamma}{s}\right)\text{sinsy} \quad , \tag{15}$$

$$G_{22} = \text{cossy} - j\left(\frac{\delta}{s}\right)\text{sinsy} \quad . \tag{16}$$

The matrix operator formalism is convenient for analysis and computer programming, especially in cases where more than one filter element is involved. This will become evident in what follows.

B. COMPARISON OF EXPERIMENT WITH ANALYTICAL MODEL FOR OFF-AXIS PLANE WAVES

The specific rotation parameter κ is given by a tensorial relationship,[7]

$$\kappa = \sum_{i,j} \rho_{ij}\, \ell_i\, \ell_j \quad , \tag{17}$$

where the ℓ_i are direction cosines of the wave propagation vector with respect to the crystallographic principal axes. In $AgGaS_2$, symmetry $\bar{4}2m$,

$$\rho_{11} = -\rho_{22} = \rho \quad , \tag{18}$$

and all other components are zero. Thus, optical activity is absent for light rays that lie anywhere in the (110) or $(1\bar{1}0)$ planes. With the configuration of Figure 2(b), where the normal to the input surface is along $<1\bar{1}0>$, κ varies as

$$\kappa = \rho\cos^2\theta\sin 2\phi \quad , \tag{19}$$

where ϕ is the angle between the $<1\bar{1}0>$ direction and the projection of the propagation vector on the (001) plane, and where θ is the angle between the propagation vector and that projection. The birefringence parameter δ varies angularly in accordance with the following relationship:

$$\delta = \frac{\pi}{\lambda}(n_e - n_o)\cos^3\theta\cos\phi$$

$$= \frac{\pi}{\lambda} C(\lambda_o - \lambda)\cos^3\theta\cos\phi \quad , \tag{20}$$

where $n_e - n_o$ is the (wavelength-dependent) full birefringence of the crystal (the difference between the extraordinary and the ordinary indices of refraction), and C is the measured rate of change of birefringence with wavelength[3,6] through the iso-index point, λ_o.

In order to establish the validity of our computer model in the most straightforward way, we first made detailed spectral transmittance measurements on $(1\bar{1}0)$ samples of $AgGaS_2$ using very narrow-field light beams for selected angles ζ off normal incidence, with beam axis in the (001) plane; i.e., $\theta = 0$. All measurements were made with no voltage applied to the crystal samples. With the input beam polarized along the optic axis, as shown in Figure 2(b), the theory predicts that the transmittance τ through a crossed polarizer is (for $Z(0) = 1$, $X(0) = 0$, $\Gamma = 0$):

$$\tau = |X(L)|^2 = |G_{12}(L)|^2$$

$$= \frac{\kappa^2 \sin^2 L \sqrt{\kappa^2 + \delta^2}}{\kappa^2 + \delta^2} \quad . \tag{21}$$

The spectrophotometric measurements were made using two identical $(1\bar{1}0)$ plates of $AgGaS_2$ of thickness L = 0.74 mm. The initial measurements were made using both plates in tandem, with optic axes parallel, so that we effectively had a single plate of thickness 1.48 mm. External angles of incidence were selected from 0° to 30° in steps of 2°. Figure 6 shows the results for four representative cases: 0°, 8°, 16°, and 24°. It is apparent from these spectral transmittances that the optical activity engenders significant coupling of polarization components in the neighborhood of the iso-index point. For modest angles of incidence, a single peak is produced; but at increasingly larger angles, additional secondary maxima materialize, while the central lobe diminishes and finally reappears strong and noticeably broader.

Figure 7 shows additional spectrometer traces for incidence angles of 12°, 20°, and 30°. Appearing with each is the corresponding computer plot based on Eq. 21 and the following values of the constants:

$$\lambda_o = 0.497 \ \mu m$$

$$\rho = 9.1 \times 10^{-3} \ \text{rad}/\mu m \ (=522° \ mm^{-1})$$

$$L = 1480 \ \mu m$$

$$C = 1.87 \ \mu m^{-1} \quad .$$

It is apparent from the agreement of these representative computer simulations that the analytical model is valid. Additional computer plots not shown also demonstrated excellent agreement with the experimental results.

The preparation of two identical $AgGaS_2$ filter elements was done in anticipation of testing a scheme proposed to counteract the undesirable coupling due to optical activity. Figure 8 illustrates the concept. The idea was to

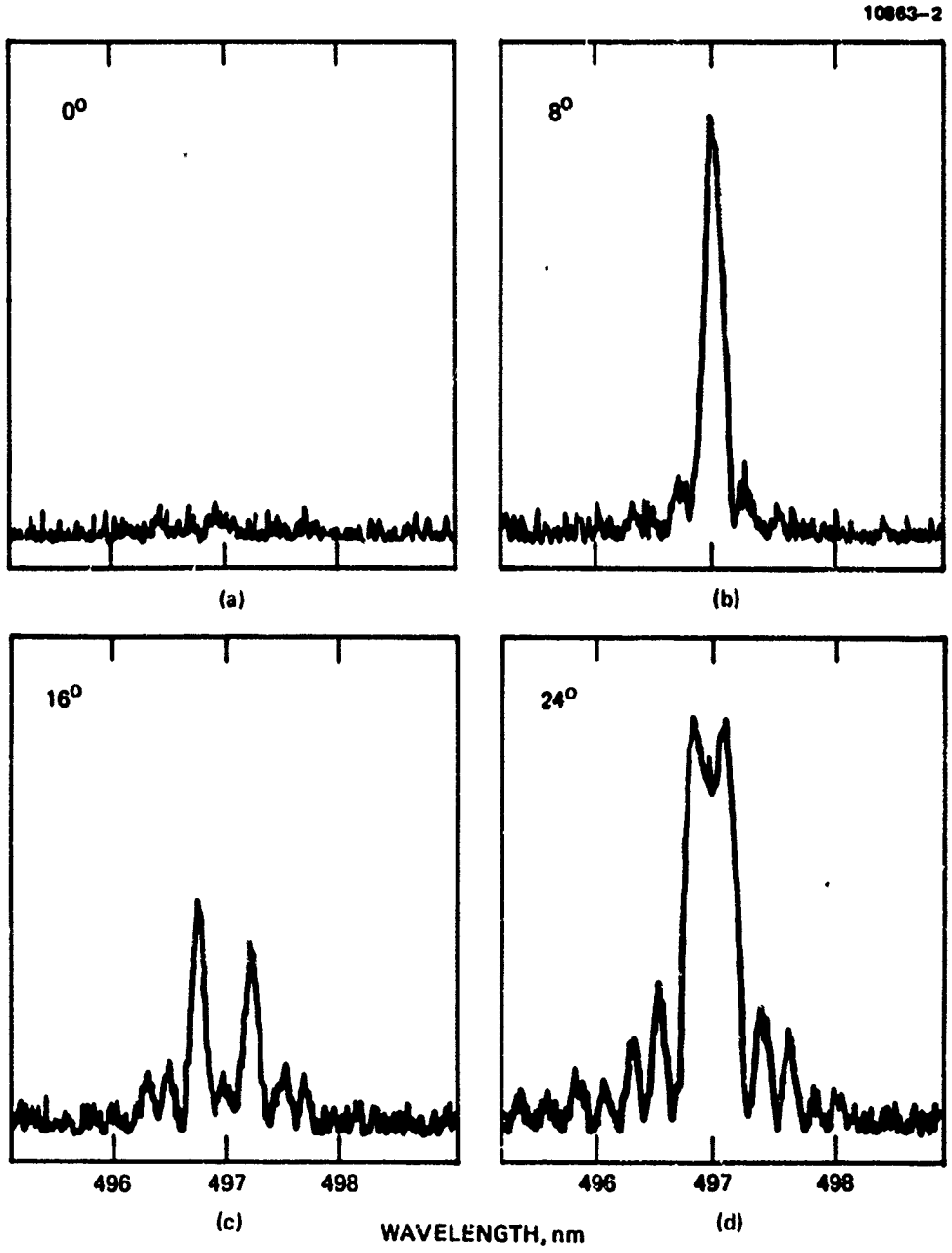

Figure 6. Sample spectrophotometer traces of filter transmission of a f/80 light cone through a 1.48-mm sample of $(1\bar{1}0)$ $AgGaS_2$ at selected angles of incidence in the (001) plane. (Configuration of Figure 2(b)).

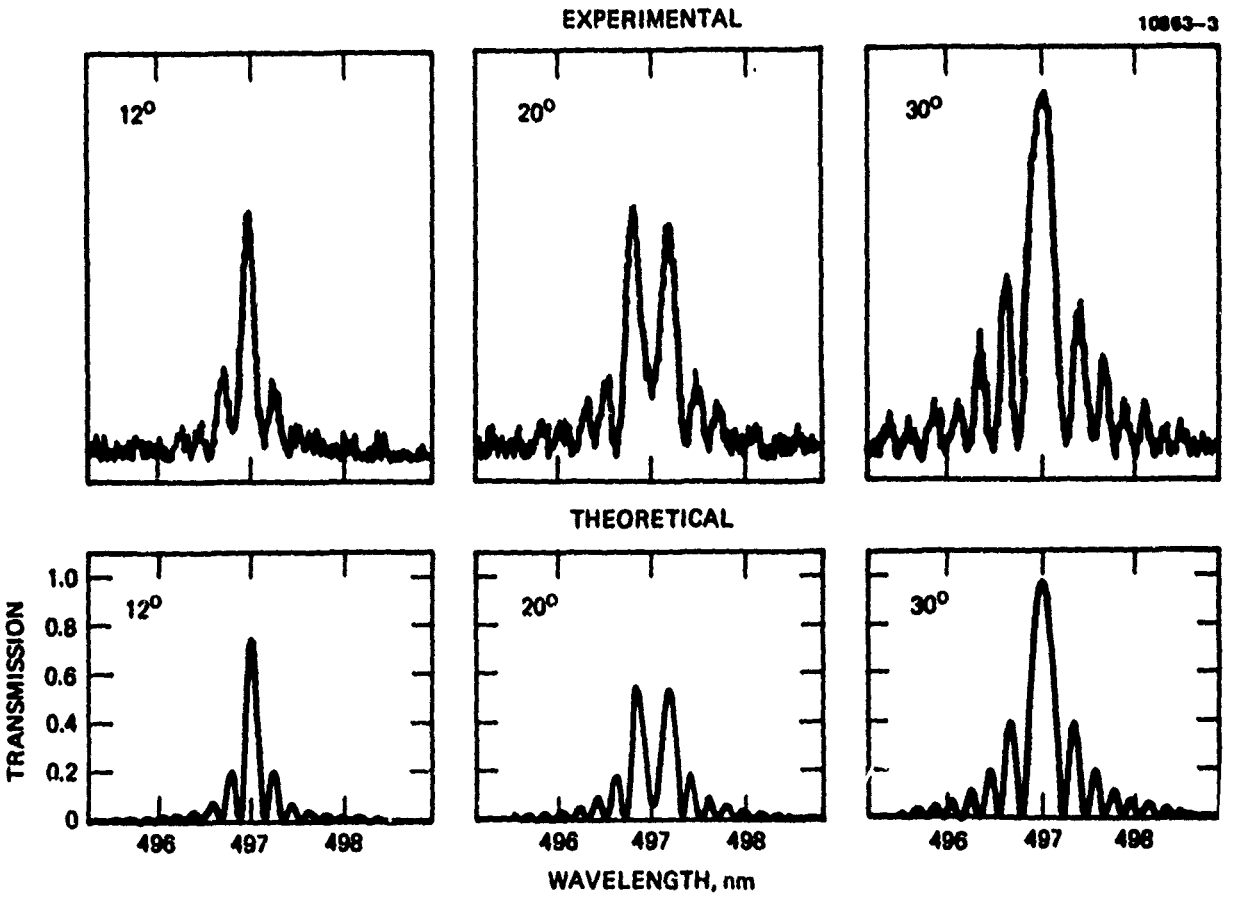

Figure 7. Additional spectrophotometer traces as in Figure 6, including corresponding computer simulations based on analytical model.

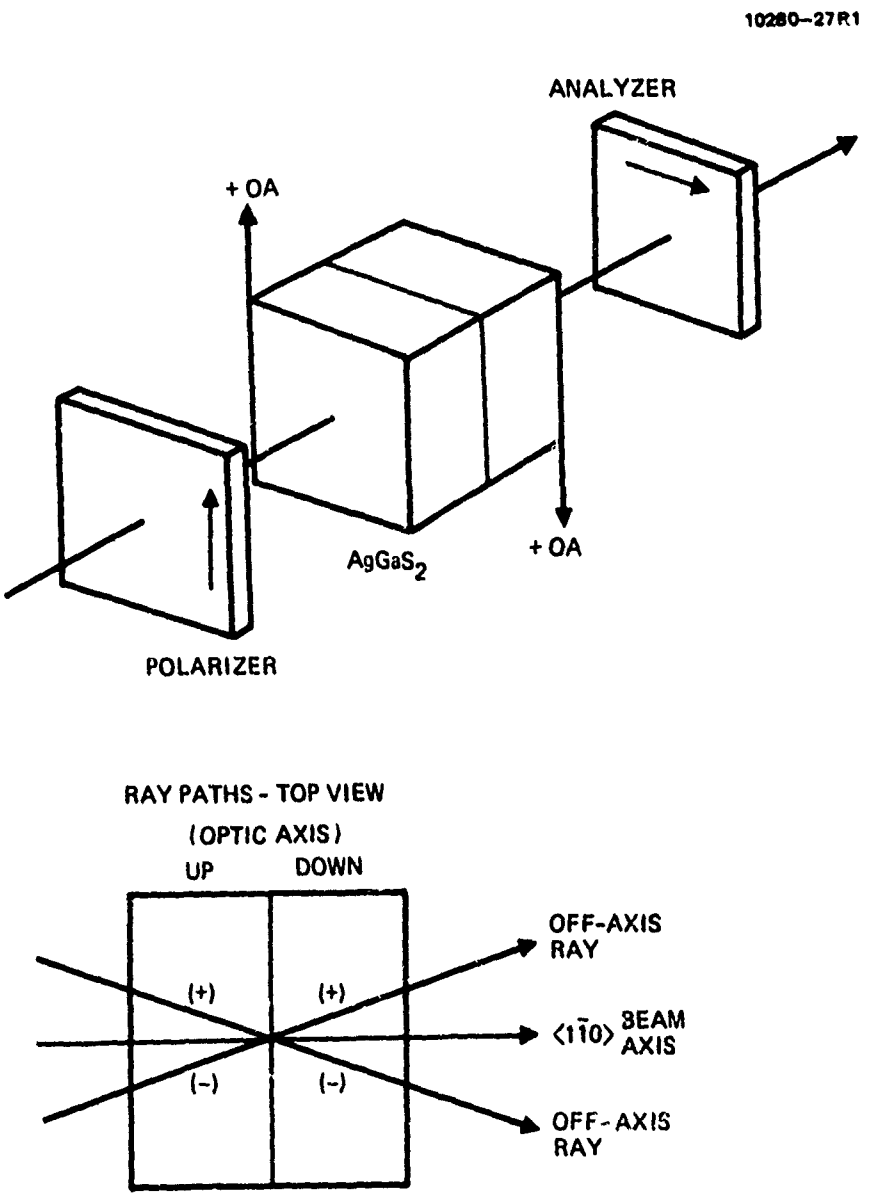

Figure 8. Two-element configuration intended for cancellation of optical coupling via optical activity in $AgGaS_2$. The scheme proved valid only at the iso-index wavelength.

operate the filter in a tandem pair of identical halves, wherein the second half is rotated through 180° about the beam axis (the $\langle 1\bar{1}0 \rangle$ direction), so that the positive optic axes of the two crystal halves are antiparallel. With this arrangement, rays off normal should experience rotatory powers of opposite sense in the two crystal elements, thereby unwinding the effects of optical activity. The concept proved valid, but only at the iso-index wavelength, at which point pure circular birefringence occurs; that is, the eigenmodes are right- and left-circularly polarized. At wavelengths away from this point, such is no longer the case — the eigenmodes being elliptically polarized — and coupling does indeed occur. The effect is illustrated in Figure 9 by two examples of experimental spectrometer traces, and accompanying computer simulations, for the cases of external incidence angles 8° and 24°. Again, excellent agreement between experimental results and the computer model is noted. It should be further noted that the transmittance at all angles of incidence is indeed zero at the iso-index wavelength, 497 nm. In formulating the analytical result, an effective matrix operator,

$$\mathcal{G} = \mathbf{G}(-\kappa, L) \cdot \mathbf{G}(\kappa, L) \quad , \tag{22}$$

was used, namely, a product of two **G** operators, wherein the sign of κ in the second was opposite to that in the first, in accordance with the experimental arrangement of the two filter elements of Figure 8. In this case, the lengths used were L = 740 μm.

A few remarks are in order at this point concerning the apparent high-selectivity experimental results of our earlier work in 1979. In the measurements made then of the dependence of filter transfer characteristics on angle of incidence, the ray propagations were limited to the (110) plane, where the optical activity is zero, as pointed out above. This constraint was due to the limited availability of crystals at that time. Since we were not fully cognizant of the presence of optical activity in $AgGaS_2$ and its effects, as detailed in this later report, the results of those experimental measurements are not representative of the filter's performance with a full, two-dimensional field of view.

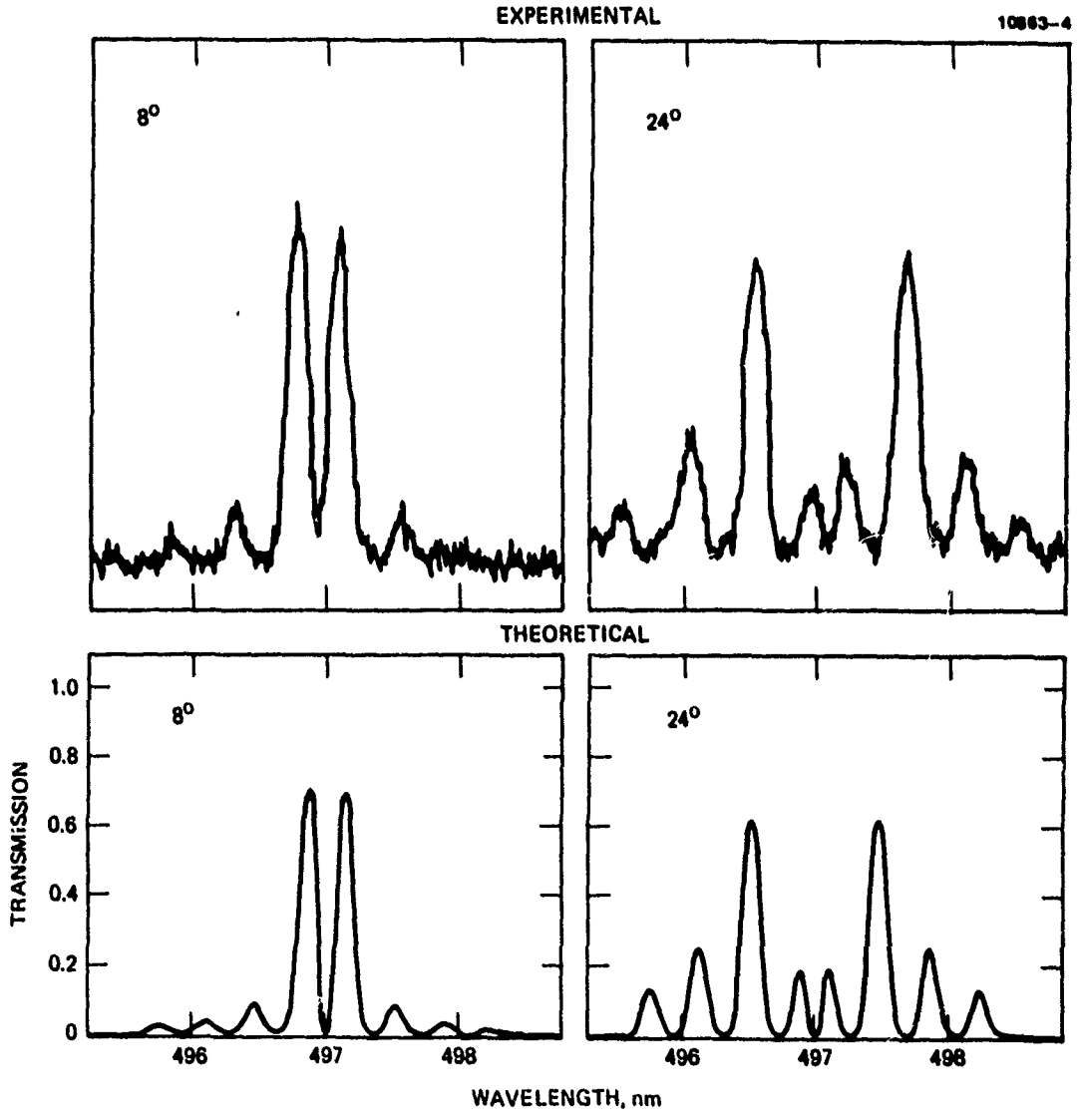

Figure 9. Examples of spectrophotometer traces for the two-element configuration of Figure 8, together with corresponding computer simulations.

Notwithstanding this fact, we will demonstrate in Section 5 several techniques that lead to a significant suppression of leakage out-of-band, for moderately wide, two-dimensional FOVs, using a novel dual-element configuration.

SECTION 5

MODELING PREDICTIONS FOR WIDE FIELDS OF VIEW

A. SINGLE ELEMENT

The analytical expression of filter transmittance, τ, used for a single element with finite FOV was a double integration of Eq. 21 over angles between limits $\pm\phi_o$, $\pm\theta_o$:

$$\tau = \frac{1}{4\theta_o\phi_o} \int_{-\theta_o}^{\theta_o} \int_{-\phi_o}^{\phi_o} |X(L)|^2 \, d\phi d\theta \quad . \tag{23}$$

Thus the input light cone is taken to have square (or rectangular) symmetry rather than cylindrical, for convenience of analysis. Because of the large refractive index of $AgGaS_2$ – n∿2.7 in the vicinity of 497 nm – maximum practical values of θ_o and ϕ_o within the crystal do not exceed ∿15°.

1. Transmittance Versus Voltage

A number of plots were generated displaying transmittance as a function of applied voltage at 497 nm, with FOV and crystal length varied parametrically. The independent variable used was a normalized voltage, v, referenced to the half-wave voltage, for which $\Gamma L = \pi/2$ at 497 nm. In $AgGaS_2$, this number is approximately 3.6 kV for a cube of material. The results showed that the maximum attainable transmission, as well as the extent of variation with v, was strongly dependent on the product L x FOV. Two extreme cases are shown in Figure 10. In Figure 10(a), L = 1.0 mm, and the FOV is f/2 (14° half angle). Here the maximum transmission approaches 100%, and the variation with voltage is great. In the case of Figure 10(b), on the other hand, where L = 5.0 mm and the FOV is f/0.5 (45° half angle), the transmittance is very insensitive to applied voltage, averaging approximately 50%. The reason for this insensitivity to voltage is that κ (see Eq. 12) is averaged over a large range of angles, contributing sizeably to optical coupling through optical activity, to such an extent that variations in Γ through v are virtually

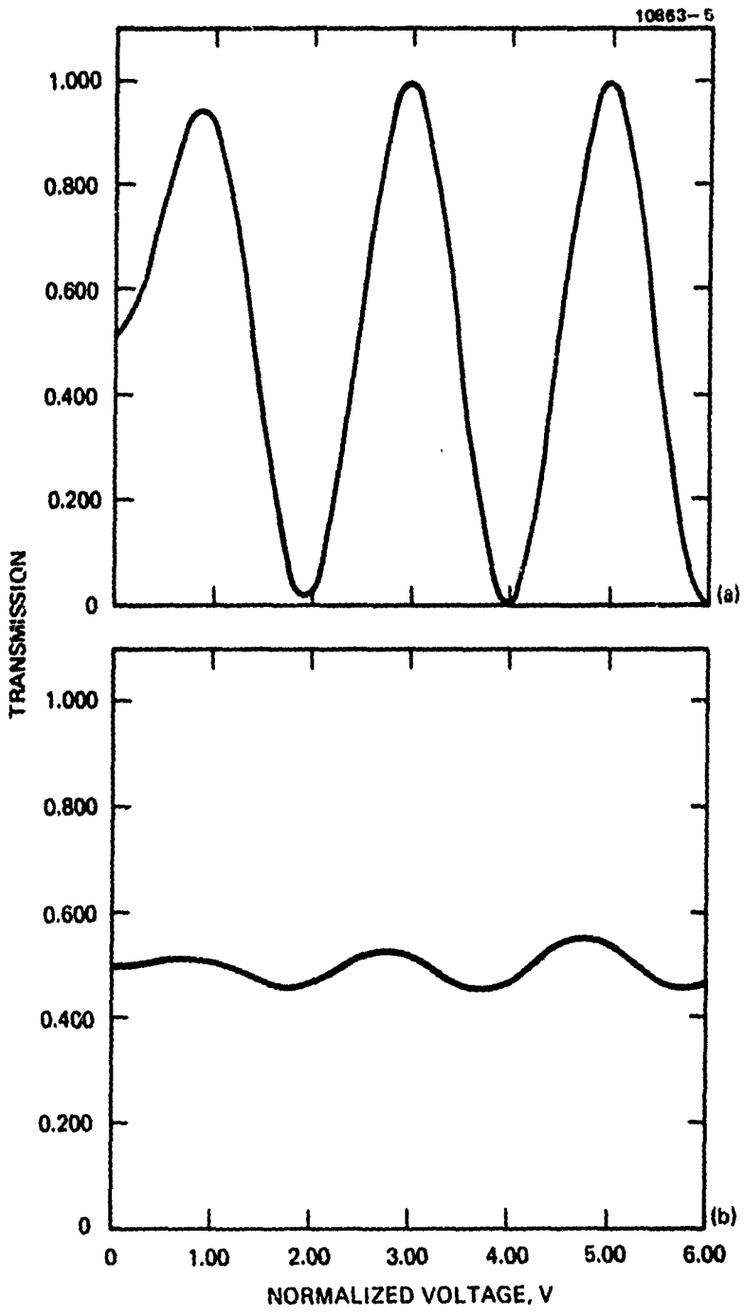

Figure 10. Theoretical transmittance of $AgGaS_2$ single-element filter at 497 nm as a function of voltage.
(a) L = 1.0 mm, FOV = f/2.0.
(b) L = 5.0 mm, FOV = f/0.5.

swamped by comparison. It is to be noted that even for the rather small FOV and small length represented in Figure 10(a), coupling through optical activity produces approximately 50% transmission with zero voltage.

The values of normalized voltage at the maxima depend slightly on the choice of L and FOV, those values being approximately 0.8, 2.8, and 4.8 for the first, second, and third maxima, respectively. In the absence of optical activity, and for very narrow FOV, these numbers would be 1, 3, and 5.

2. Transmittance Versus Wavelength

Through computer simulation, we extensively examined the filter transfer characteristics as a parametric function of length, voltage, and FOV. It was found that for crystal lengths of a few millimeters, the effects of optical activity on the filter passband are negligible, so long as the FOV is smaller than about f/10. For larger FOVs and crystal lengths, the main lobe of the filter transfer characteristic broadens, eventually merging with the first-order sidelobes; and out-of-band transmission becomes excessive.

Figure 11(a) shows an ideal filter passband characteristic for a $AgGaS_2$ element of 1.5 mm length, with v = 1.0 and f/∞. The 3 dB bandwidth is 1.4 Å. The result of opening up the FOV to f/0.5 is shown in Figure 11(b). It is seen that the peak transmission has dropped to 53%, which is maximum at a reduced normalized voltage of 0.75, and that the first few sidelobes are broadened into a sizeable pedestal. Some improvement in peak transmission can be had by selecting the next higher voltage maximum at v = 2.80, as shown in Figure 12(a); but broadening of the main lobe results, as well as an increase in out-of-band transmission. A further degradation of selectivity occurs at the third maximum, v = 4.70, as seen in Figure 12(b).

It is well known that selectivity can be increased by increasing the crystal length,[3] in the absence of optical activity. In the case of $AgGaS_2$, however, out-of-band polarization coupling due to optical activity also increases with length, thereby thwarting attempts to decrease filter bandwidth in wide-FOV operation. This effect is illustrated dramatically in Figure 13, showing passband characteristics of a 5 mm sample at the first (v = 0.78) and second (v = 2.77) voltage maxima, for a f/0.5 field of view.

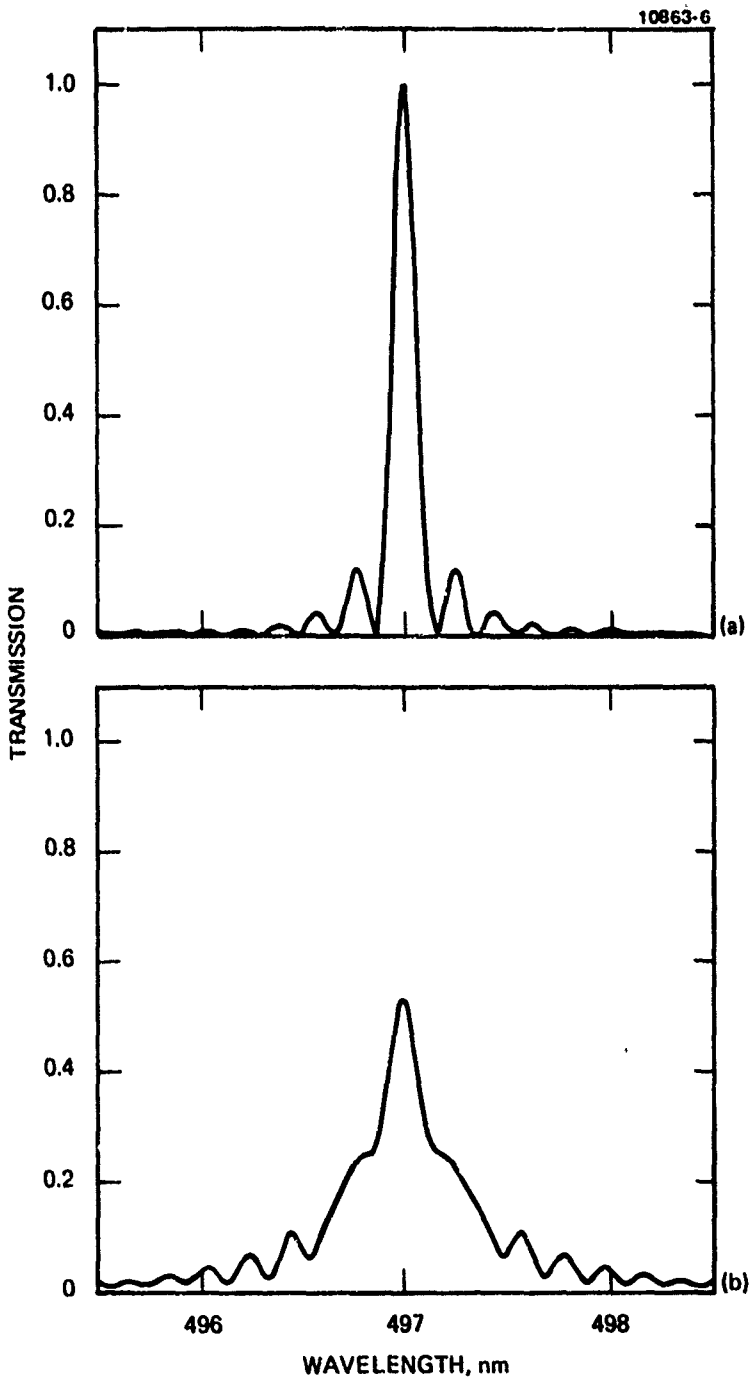

Figure 11. Theoretical transfer characteristics of a 1.5-mm $AgGaS_2$ filter.
(a) $v_1 = 1.0$, FOV = f/∞.
(b) $v_1 = 0.75$, FOV = f/0.5.

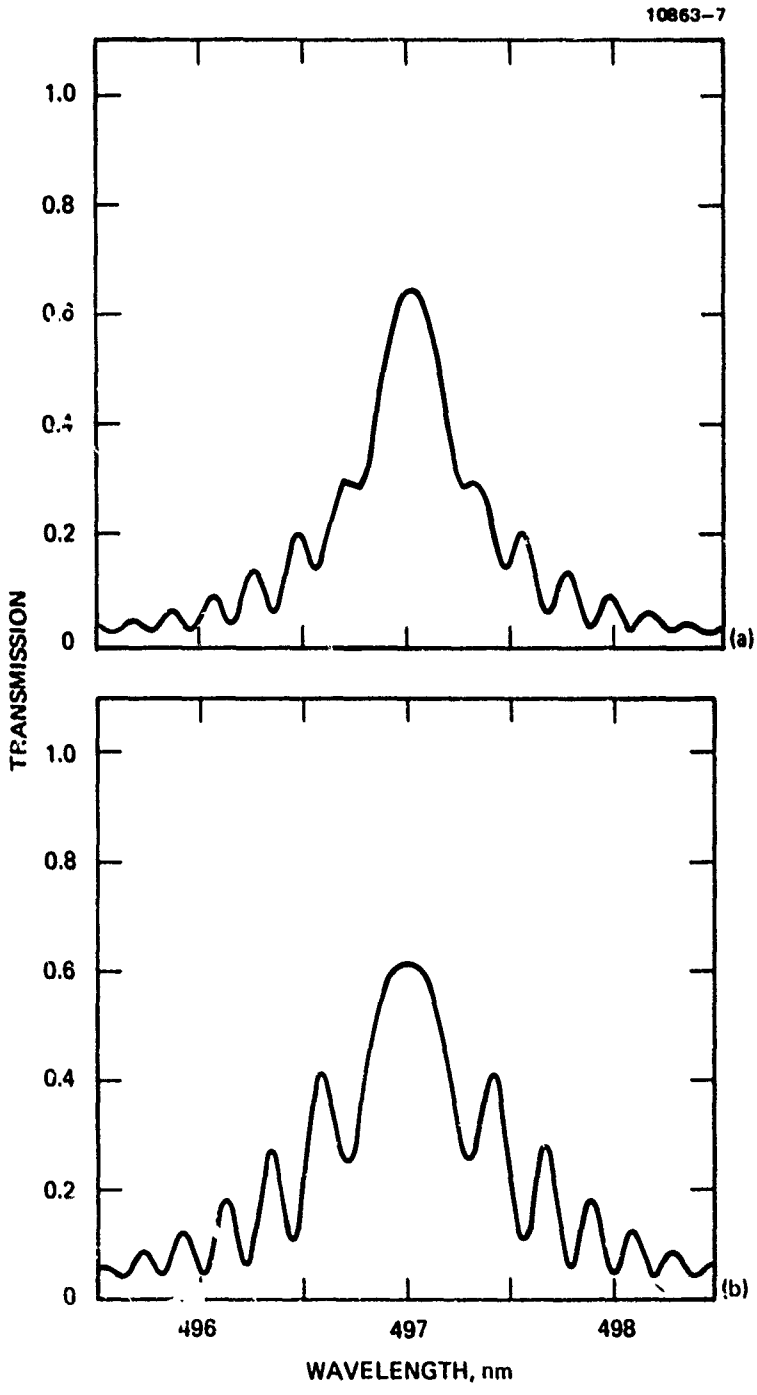

Figure 12. Theoretical transfer characteristics of a 1.5-mm $AgGaS_2$ filter. (a) v_2 = 2.8, FOV = f/0.5. (b) v_3 = 4.7, FOV = f/0.5.

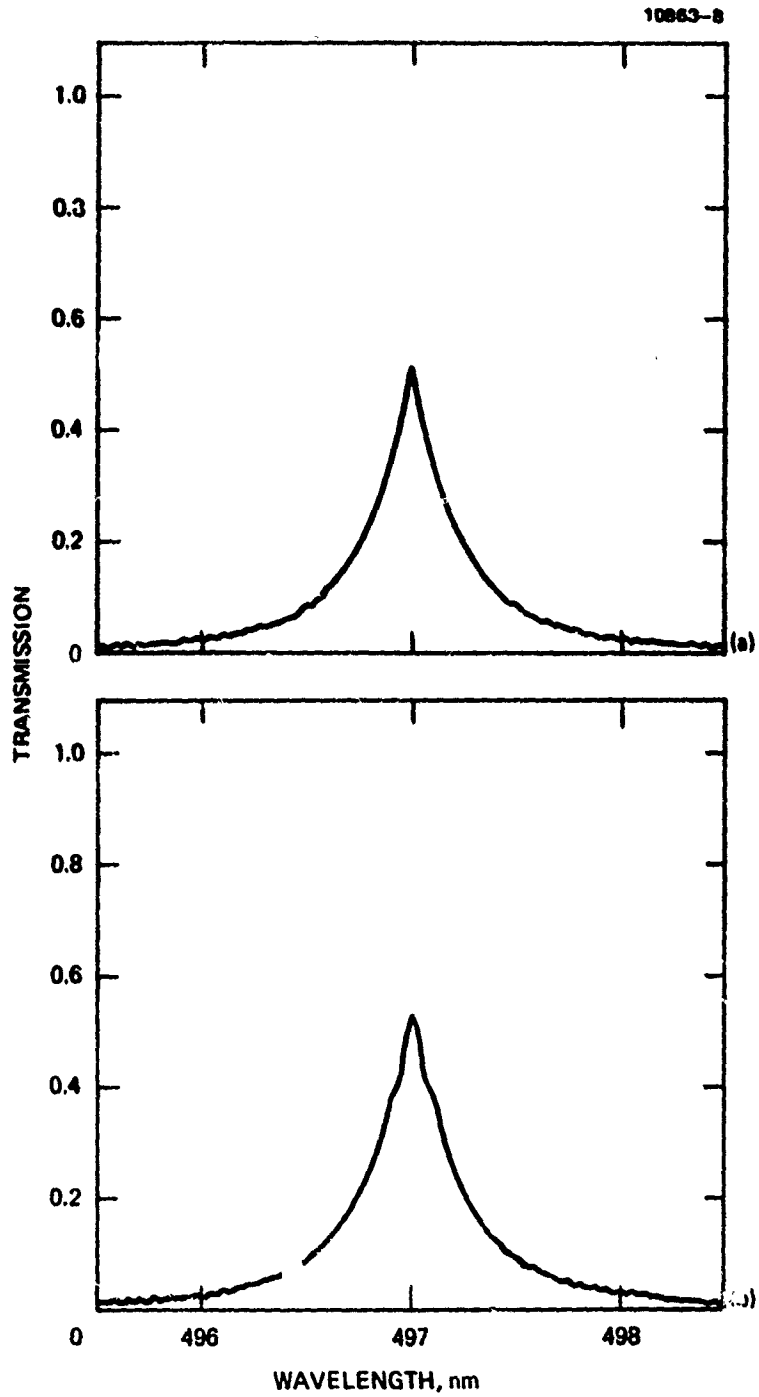

Figure 13. Theoretical transfer characteristics of a 5.0-mm $AgGaS_2$ filter. (a) $v_1 = 0.78$, FOV = f/0.5, (b) $v_2 = 2.77$, FOV = f/0.5.

Sidelobe structure is virtually non-existent; and what appears is effectively an envelope function, characterized by substantial out-of-band transmission.

3. Peak Transmittance Versus Crystal Length

A comprehensive picture of maximum filter transmission can be seen in the curves of Figure 14. There we show the variations in peak transmission of a $AgGaS_2$ filter element as a function of crystal length for four different fields of view: f/0.5, f/1.0, f/1.5, and f/2.0. The four sets of curves correspond to four voltage choices: $v = 0$, and $v = v_1$, v_2, and v_3 producing the first three transmittance maxima. What is evident from these curves is that for lengths in excess of about 3 mm the maximum transmission is virtually insensitive to variations in length, FOV, and voltage. Only at the shorter lengths do both voltage and FOV have a significant influence on filter transmission. The curves of Figure 14 give no information, of course, about bandwidth characteristics.

4. Filter Bandwidth Versus Crystal Length

From the computer data generated in connection with analysis of the above parametric dependencies, the bandwidth curves of Figure 15 were plotted. In this set of curves, the independent variable is again crystal length, with four FOVs and four voltages selected parametrically as above. The increasing width of the passband with increasing FOV is an obvious trend. More significantly, however, a minimum bandwidth is indicated for a crystal length in the vicinity of 3 mm. This adds further emphasis to the remarks made earlier concerning the increasing influence of optical activity with increasing crystal length. It is concluded from Figure 15 that a minimum bandwidth of $\sim$2 Å is achievable with an f/1 field and $\sim$1 Å with an f/2 field.

B. DUAL ELEMENT FOR ENHANCED SELECTIVITY

A novel dual-element filter configuration[9] was conceived that provides substantial passband narrowing and reduction in out-of-band transmission, with comparable voltages applied. The configuration can take several forms as shown below, one of which exhibits a dramatic suppression of sidelobe

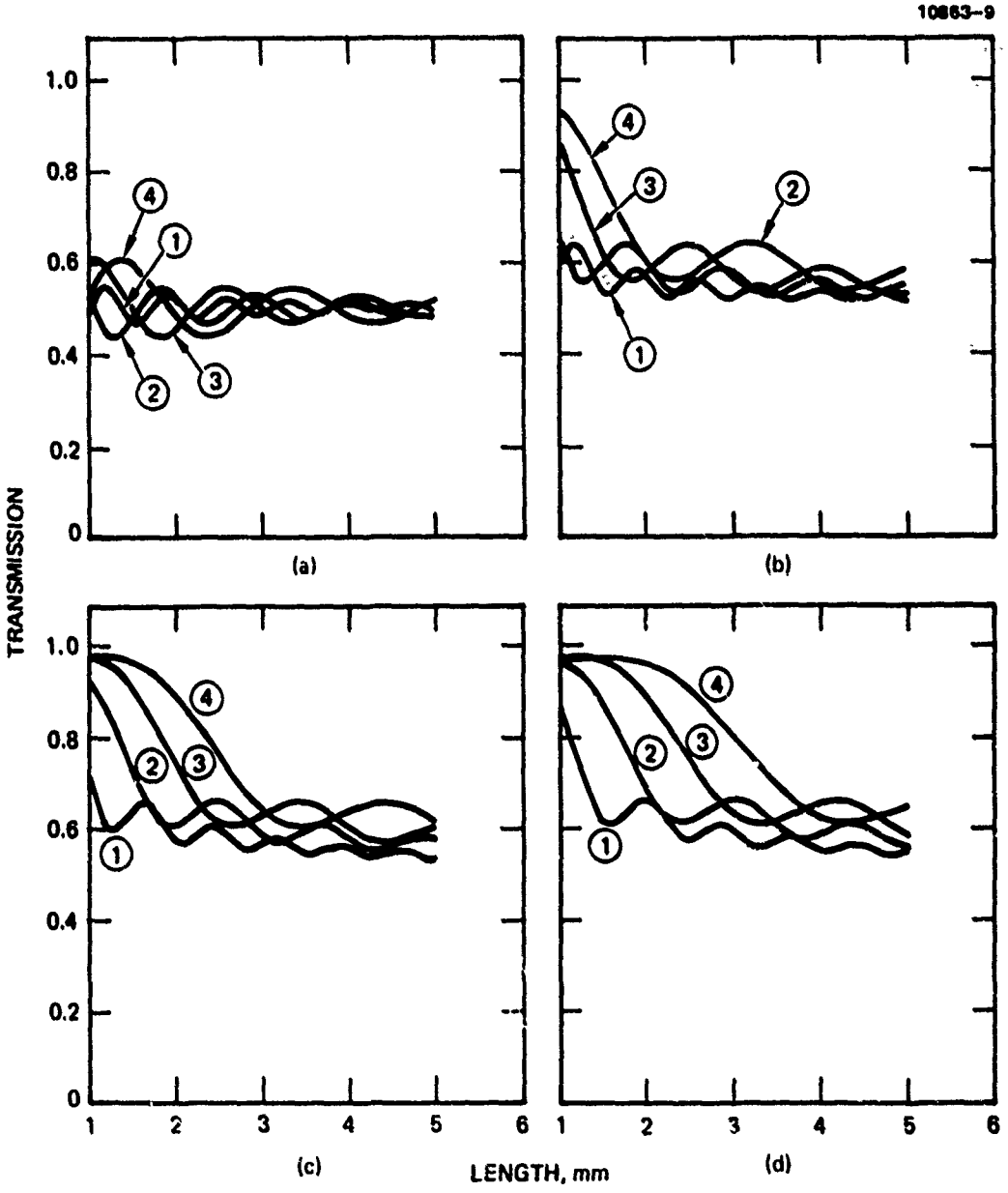

Figure 14. Theoretical peak transmittance at 497 nm of $AgGaS_2$ filter as a function of length. (a) v = 0; (b) $v = v_1$; (c) $v = v_2$; (d) $v = v_3$. Legend: ① = f/0.5, ② = f/1.0, ③ = f/1.5, ④ = f/2.0.

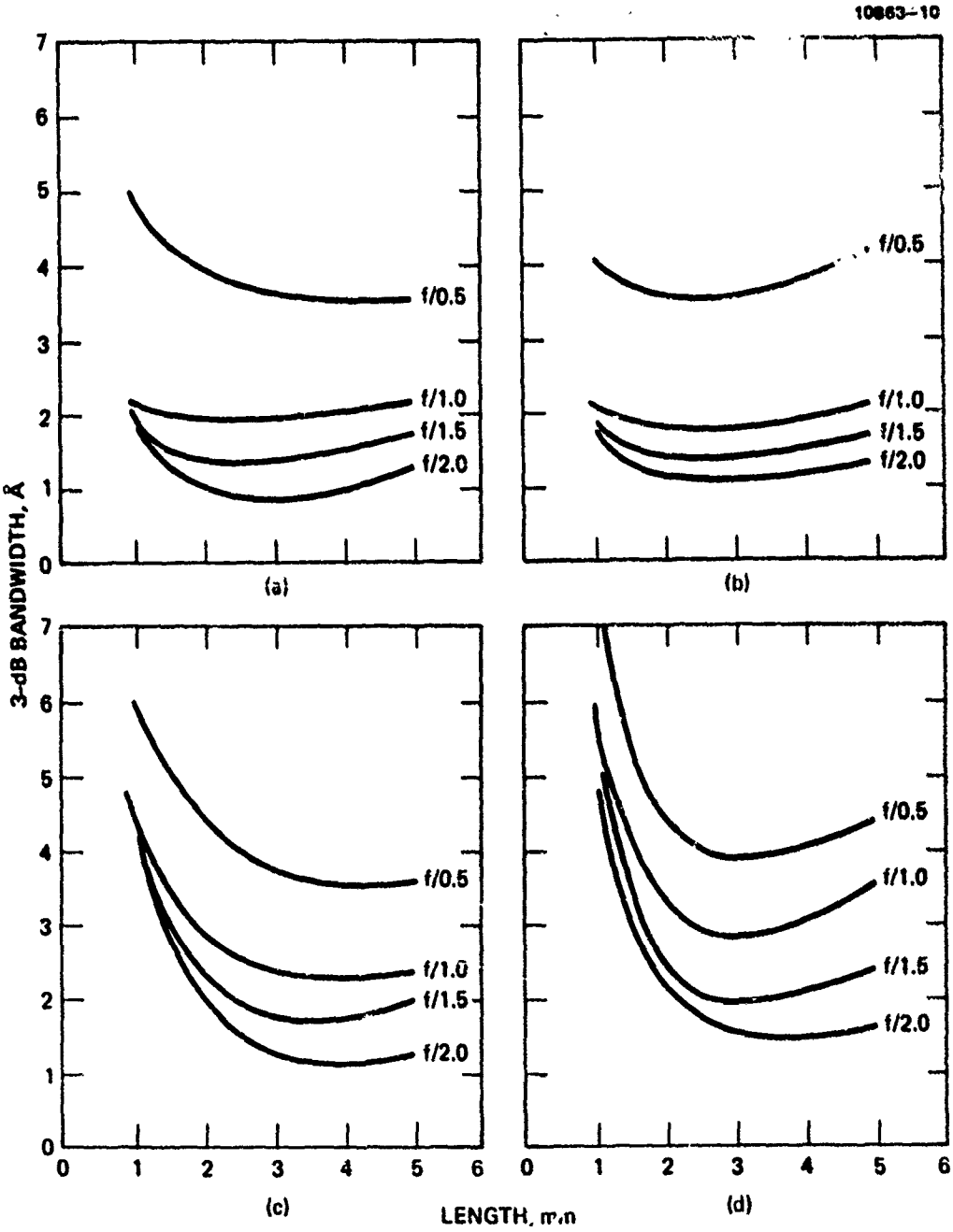

Figure 15. Theoretical 3-dB bandwidth of $AgGaS_2$ filters as a function of length. (a) v = 0; (b) v = v_1; (c) v = v_2; (d) v = 4_3.

structure. There are limits, however, to the minimum passband achievable by these means; and the technique works best with relatively short lengths of crystal, and with FOVs smaller than ∿f/1.

1. Basic Configuration

The scheme as initially proposed consists of operating the filter as a tandem pair of identical crystal elements, as shown in Figure 16, wherein the second element – following a crossed polarizer – is rotated through 90° about the axial beam axis (the $\langle 1\bar{1}0 \rangle$ direction), so that the optic axes (O.A.) of the two crystal elements are orthogonal to each other. We have shown that the optical activity in $AgGaS_2$ exhibits its strongest effect in the (001) plane, varying about the $\langle 1\bar{1}0 \rangle$ direction as $\sin 2\phi$. Moreover, the optical activity is zero for light rays anywhere in the (110) plane. Thus, with the configuration of Figure 16, off-axis rays in or near the (001) plane in the first element, for which the optical activity is large, will traverse regions of the second element where optical activity is minimal. They will thus be filtered out effectively by the near-ideal filter characteristics of the second element with respect to those particular rays. The presence of the central crossed polarizer will, in and of itself, provide additional selectivity because the spectral input to the second filter element is preselected thereby.

10863-11

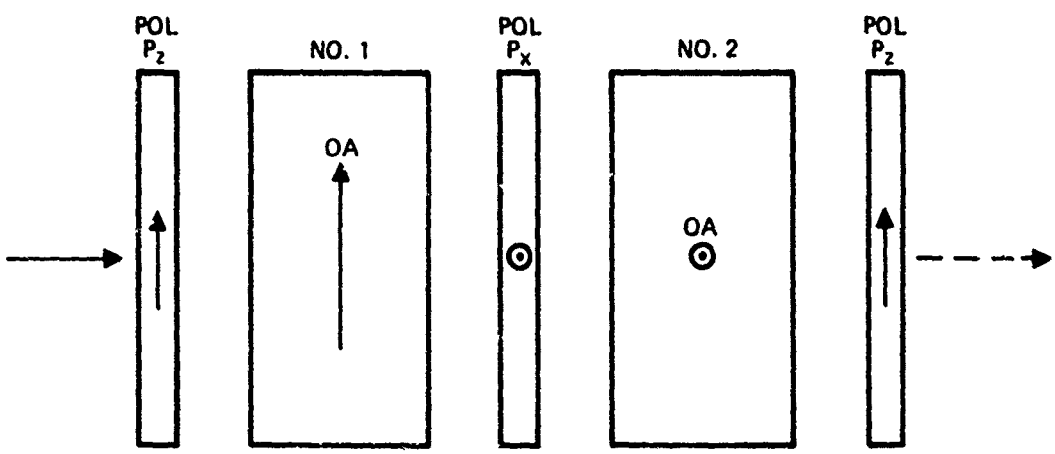

Figure 16. Proposed dual-element iso-index filter for suppressing out-of-band transmissions.

The effectiveness of the proposed dual-element configuration in suppressing out-of-band transmission is illustrated in Figure 17. The transmission characteristics shown in Figure 17(a) are those for a single-element $AgGaS_2$ filter of 1.5 mm length, for input light cones of 16° half-angle (f/1.8), and 24° half-angle (f/1.1). The indicated voltages correspond to the second transmission maximum. Figure 17(b) shows the corresponding filter characteristics of the dual-element design. It is quite apparent from these illustrations that the excessive sidelobe structure is substantially reduced without seriously impairing the maximum transmittance of the filter's main lobe.

The general operator equation for this dual-element configuration is

$$\vec{E}(2L) = \mathbf{G}(\kappa_2,\delta_2,L_2)\cdot\mathbf{P}\cdot\mathbf{G}(\kappa_1,\delta_1,L_1)\cdot\vec{E}(0) \quad , \tag{24}$$

where

$$\kappa_1 = \rho\cos^2\theta\sin2\phi \quad , \tag{25}$$

$$\kappa_2 = \rho\sin2\theta\cos\phi \quad , \tag{26}$$

$$\delta_1 = \frac{\pi}{\lambda}C(\lambda_o - \lambda)\cos^3\theta\cos\phi \quad , \tag{27}$$

$$\delta_2 = -\frac{\pi}{\lambda}C(\lambda_o - \lambda)\cos\theta\cos^3\phi \quad , \tag{28}$$

$$\mathbf{P} \equiv \begin{pmatrix} P_x & 0 \\ 0 & P_z \end{pmatrix} \quad , \tag{29}$$

and $2L \equiv L_1 + L_2$. The particular functional dependencies of κ_2 and δ_2 result from rotation of the second filter element through 90°. With the orientation of Figure 16, the resulting transmittance characteristics shown in Figure 17(b) are represented by

$$\tau = \frac{1}{4\theta_o\phi_o}\int_{-\theta_o}^{\theta_o}\int_{-\phi_o}^{\phi_o}|Z(2L)|^2 d\phi d\theta \quad , \tag{30}$$

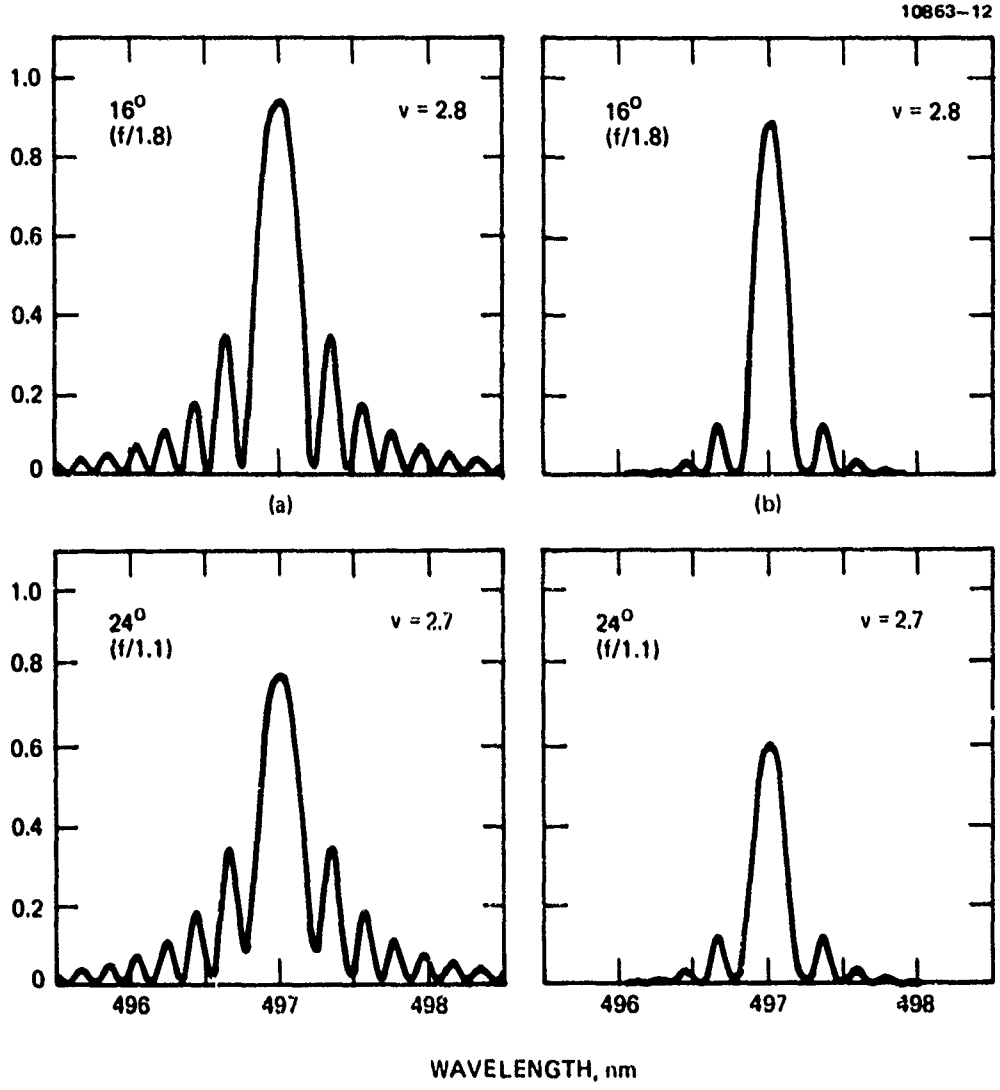

Figure 17. Computer simulations of excess sidelobe suppression by means of proposed dual-element $AgGaS_2$ filter. (a) single element; (b) dual element. (Configuration of Figure 16.) L = 1.5 mm.

where

$$P_x = 1,\ P_z = 0,\ L_1 = L_2 = 1.5 \text{ mm}.$$

2. Unequal Lengths

By using crystal elements of unequal length, we were able to effect a further, dramatic reduction in sidelobe transmission. The lengths were so chosen that the first few maxima of the sidelobes of one element coincide as nearly as possible with the zeroes of the other element. The results are illustrated in Figure 18 for a f/1.8 FOV, with L_1 = 1.5 mm, v_1 = 2.8, L_2 = 1.1 mm, and v_2 = 2.9. Figure 18(a) shows the individual transfer characteristics (Eq. 23) superimposed. Figure 18(b) is the resultant dual-element transmittance (Eq. 30).

3. Unequal Voltages

A similar effective suppression of sidelobe levels was found to result if different voltages were used, corresponding to first and second maxima, instead of different lengths. These results are shown in Figure 19 for an f/1.0 FOV, with L_1 = 1.0 mm, v_1 = 0.70, L_2 = 1.0 mm, and v_2 = 2.8. With this arrangement, a reasonably good peak transmission of 62% was achieved only for the relatively short lengths of $\sim$1.0 mm.

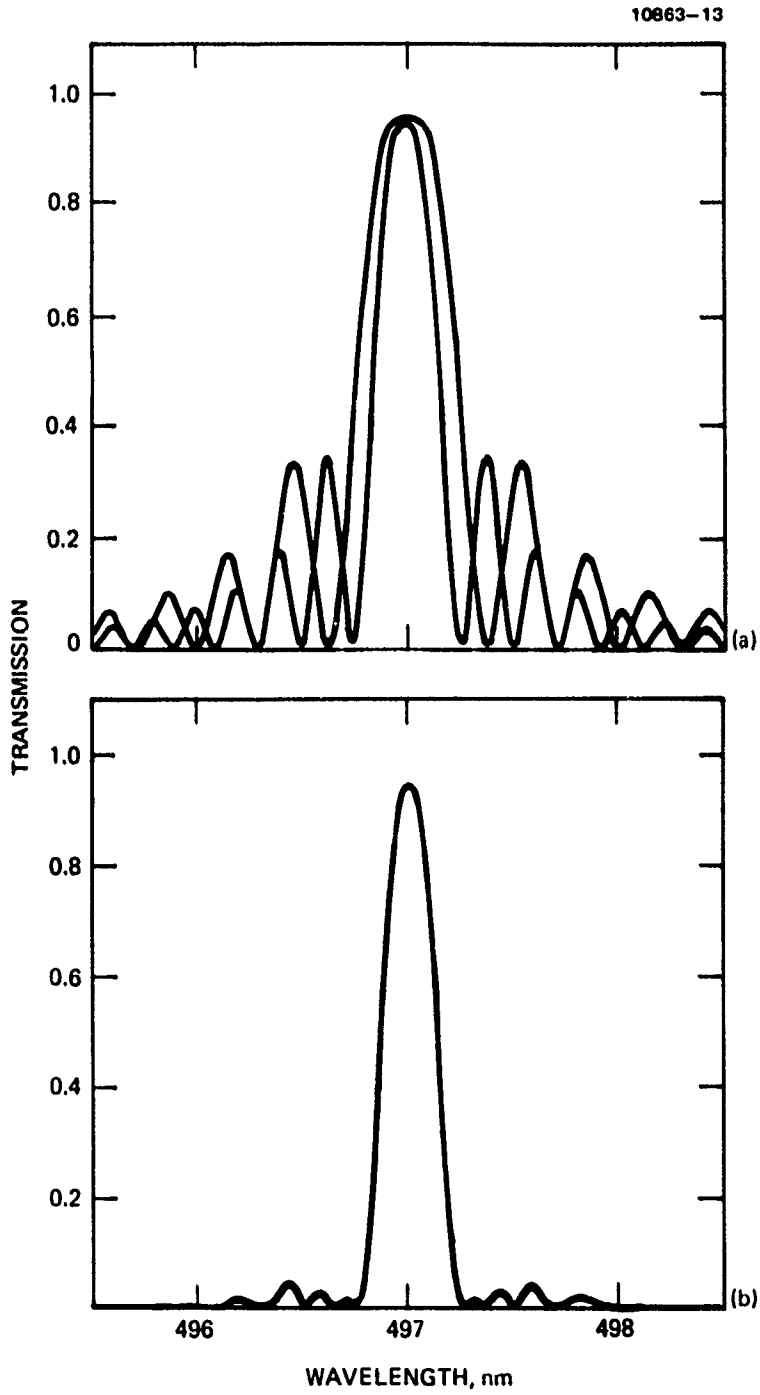

Figure 18. Computer simulations of $AgGaS_2$ dual-element filter transfer characteristic using unequal element lengths: L_1 = 1.5 mm, L_2 = 1.1 mm. (a) single elements, superimposed; (b) dual element. FOV = f/1.8; $v = v_2$.

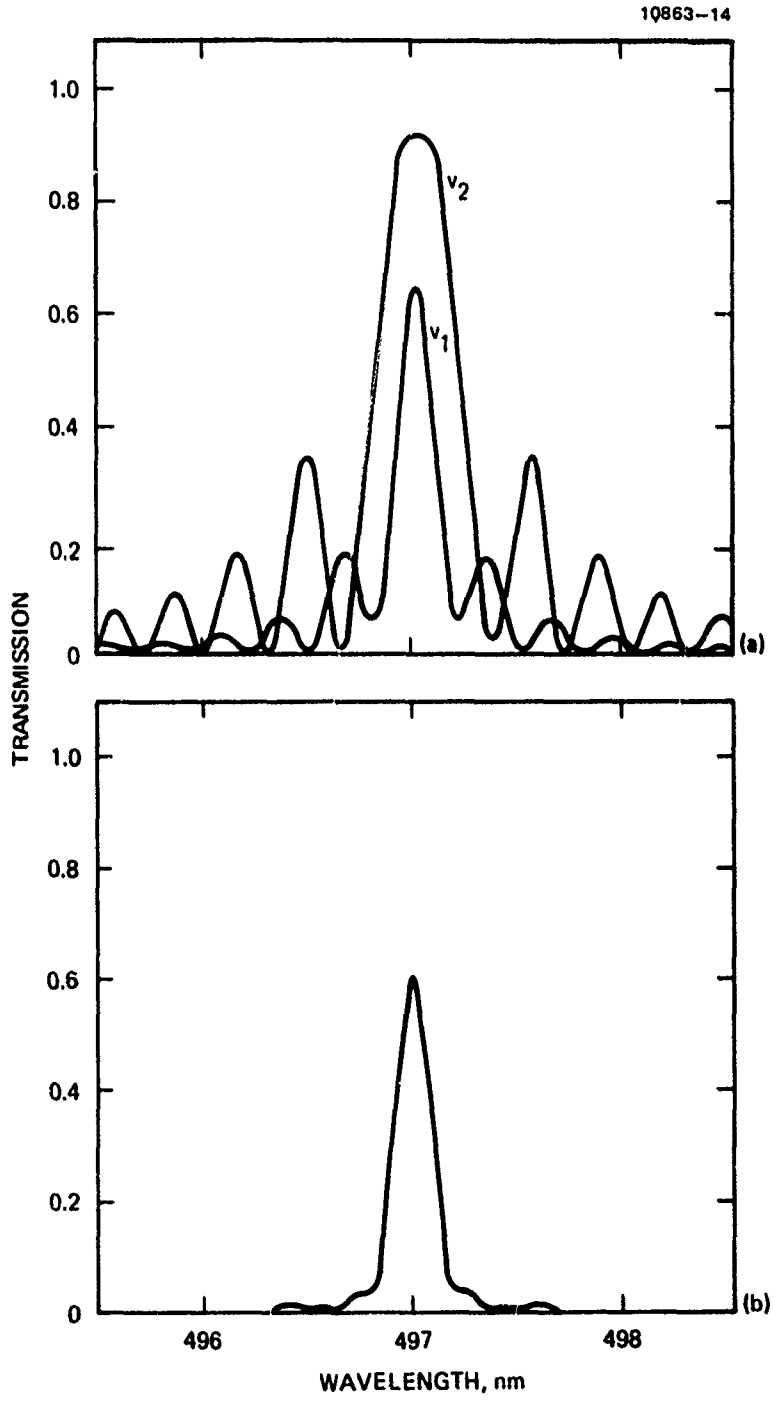

Figure 19. Dual-element transfer characteristics using equal lengths, L = 1.0 mm, but unequal voltages. (a) single elements, superimposed; (b) dual element. FOV = f/1.0. v_1 = 0.70, v_2 = 2.8.

SECTION 6

CONCLUSIONS AND RECOMMENDATIONS

The performance of $AgGaS_2$ iso-index coupled-wave electro-optic filters in wide FOV operation has been characterized in detail, both theoretically and experimentally. The principal conclusions of this program are: (1) The effect of optical activity on the filter passband is negligible for input light cones smaller than ∿f/10 (3° half-angle). (2) For larger FOVs, the main lobe of the filter transfer characteristic broadens considerably, and increased out-of-band transmission occurs. (3) At very large FOVs (∿f/0.5), the peak transmittance approaches 50%, virtually independent of applied electric field. (4) The effects of optical activity override attempts to narrow the passband by increasing filter length, resulting in an optimum crystal length of about 3 mm and a minimum passband of about 2 Å for an f/1 FOV (1 Å for f/2 FOV). (5) Significant reduction in out-of-band transmission was shown to result from using a novel dual-element arrangement with intervening crossed polarizer.

There is ample evidence from this and our preceding blue/green contract studies that the iso-index coupled-wave filter concept is valid, basically simple in structure, and worth pursuing further. It has become similarly evident, however, that the initial excitement over $AgGaS_2$ as a highly selective filter material has been significantly lowered by virtue of the limiting effects due to the sizeable optical activity present in this material. We feel that much useful work remains to be carried out in this area in the general field of synthesis of new crystalline materials, such as (Cd,Zn)S, that exhibit the iso-index characteristic, but where optical activity is not present (see Figure 5). Additional effort of a theoretical nature aimed at exploring the unique materials characteristics that give rise to the property of dispersive birefringence is also recommended.

REFERENCES

1. J.F. Lotspeich, "Iso-index filter technology," presented at the Strategic Blue/Green Optical Communications Program Review, Office of Naval Research, Arlington, Virginia, May 1979.

2. J.F. Lotspeich, "Iso-index coupled-wave electro-optic filter," presented at the IEEE/OSA Conference on Laser Engineering and Applications, Washington, D.C., May - June 1979.

3. J.F. Lotspeich, "Iso-index coupled-wave electro-optic filter," IEEE J. Quantum Electron. QE-15, 904-907 (Sept. 1979).

4. C.H. Henry, "Coupling of electromagnetic waves in CdS," Phys. Rev. 143, 627-633 (Mar. 1966).

5. J.P. Laurenti, K.C. Rustagi, and M. Rouzeyre, "Optical filters using coupled light waves in mixed crystals," Appl. Phys. Lett. 28, 212-213 (Feb. 1976).

6. G.D. Boyd, H. Kasper, and J.H. McFee, "Linear and nonlinear optical properties of $AgGaS_2$, $CuGaS_2$, and $CuInS_2$, and theory of the wedge technique for the measurement of nonlinear coefficients," IEEE J. Quantum Electron. QE-7, 563-573 (Dec. 1971).

7. J.F. Nye, Physical Properties of Crystals (Oxford, 1976); Chap. 14.

8. M.V. Hobden, "Optical activity in a non-enantiomorphous crystal: $AgGaS_2$," Acta Crystallogr. 24A, 676-680 (1968).

9. J.F. Lotspeich and R.L. Abrams, Hughes Research Laboratories, Patent pending.

APPENDIX A

COUPLED-MODE ANALYSIS OF OPTICAL ACTIVITY IN UNIAXIAL CRYSTALS

We consider the problem of light with wave vector $\vec{k}$ propagating along a given direction in a crystal which we will call y, not to be confused with the crystallographic <010> axis. The crystal is both birefringent and optically active. We can solve for the "ordinary" and "extraordinary" eigenmodes with no optical activity. These are our zero-order unperturbed eigenmodes shown in Figure A.1. Here the crystal coordinate system is labeled x',y',z'.

The solution for the unperturbed modes is assumed to be known, and leads to two waves with $\vec{D}$ vectors along x and z and propagation constants,

$$k_x = \frac{\omega}{c} n_x \text{ and } k_z = \frac{\omega}{c} n_z \quad ,$$

where

$$n_x = n_o \quad ,$$

and

$$\frac{1}{n_z^2} = \frac{\cos^2\theta}{n_e^2} + \frac{\sin^2\theta}{n_o^2} \quad .$$

The effect of optical activity is to introduce off-diagonal elements ε_{xz}, which induce a new polarization $\vec{P}_{pert}$, where

$$\vec{P}_{pert} = \varepsilon_o \begin{vmatrix} 0 & 0 & ja \\ 0 & 0 & 0 \\ -ja & 0 & 0 \end{vmatrix} \begin{vmatrix} E_x \\ E_y \\ E_z \end{vmatrix} \quad .$$

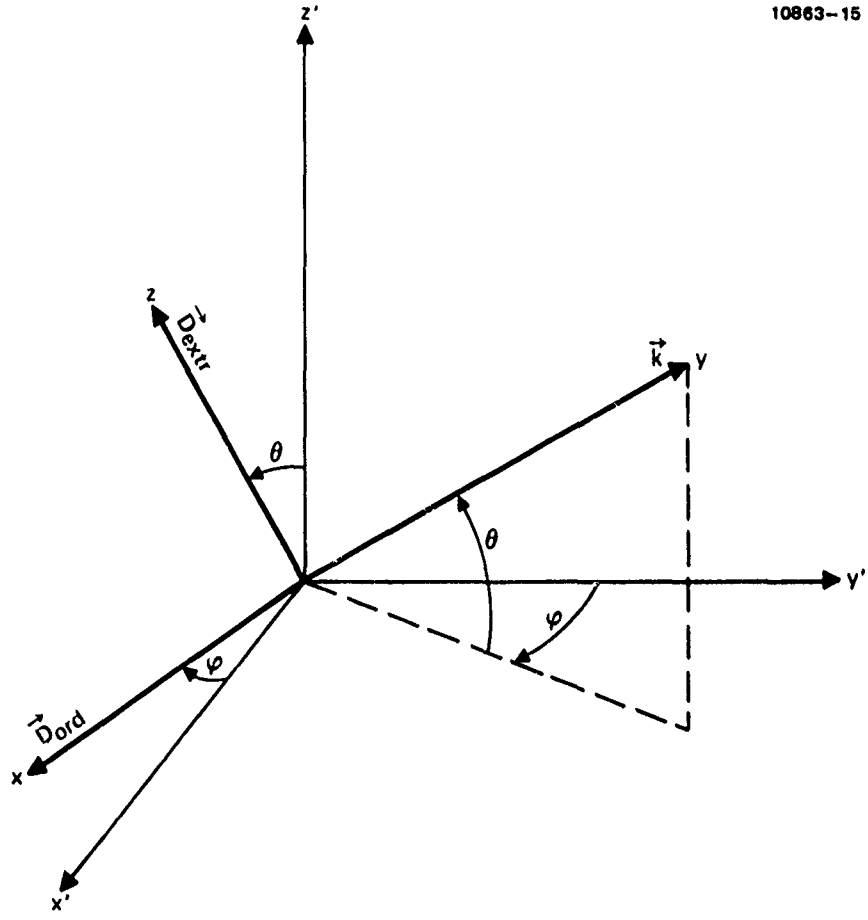

Figure A-1. Coordinate axes systems used to define crystal orientation and wave propagation vectors in optically-active uniaxial crystal.

We use $\vec{P}_{pert}$ in the wave equation,

$$\nabla^2 \vec{E} = \mu\varepsilon \frac{\partial^2 \vec{E}}{\partial t^2} + \mu \frac{\partial^2}{\partial t^2} \vec{P}_{pert} \quad . \tag{A-1}$$

The extraordinary and ordinary waves satisfy Eq. A-1 with $\vec{P}_{pert} = 0$. We can thus take the field in the presence of the perturbation as the sum of the eigenmodes, but with y-dependent amplitudes:

$$\vec{E}(x,y,z,t) = \hat{x}\, E_x(y)\, e^{j(\omega t - k_x y)} + \hat{z}\, E_z(y)\, e^{j(\omega t - k_z y)} + \text{c.c.} \quad . \tag{A-2}$$

We put A-2 into A-1, assuming

$$\left| \frac{\partial^2 E_{x,z}}{\partial y^2} \right| << \left| k_{x,z}^2 E_{x,z} \right| \quad ,$$

and obtain

$$\frac{dE_x}{dy} = - \frac{j\omega^2 \mu_o}{k} (P_{NL})_x\, e^{jk_x y} \quad , \tag{A-3}$$

and

$$\frac{dE_z}{dy} = - \frac{j\omega^2 \mu_o}{k} (P_{NL})_z\, e^{jk_z y} \quad . \tag{A-4}$$

The form of $\vec{P}_{NL}$ for an optically active medium (See Appendix C) is

$$\vec{P}_{NL} = \varepsilon_o \begin{vmatrix} 0 & ja \\ -ja & 0 \end{vmatrix} \begin{vmatrix} E_x \\ E_z \end{vmatrix} \quad , \tag{A-5}$$

which, when used in A-3 and A-4, gives

$$\frac{dE_x}{dy} = \frac{k_o a}{n} e^{-j(k_z-k_x)y} E_z \quad ,$$

$$= \kappa_{xz} e^{-j(k_z-k_x)y} E_z \quad ,$$

$$\frac{dE_z}{dy} = -\frac{k_o a}{n} e^{+j(k_z-k_x)y} E_x \quad ,$$

$$= \kappa_{zx} e^{j(k_z-k_x)y} E_x \quad , \qquad \text{(A-6)}$$

and

$$\kappa_{xz} = -\kappa_{zx} = \frac{k_o a}{n} \quad .$$

We can diagonalize Eq. A-6 (see Appendix B) to find the eigenmodes (where $\kappa = k_o a/n$, $\delta = 1/2\ (k_z - k_x)$, $s = \sqrt{\kappa^2 + \delta^2}$).

The first eigenmode is

$$\left|\begin{matrix} \bar{E}_x(y) \\ E_z(y) \end{matrix}\right|_1 = \left|\begin{matrix} E_x e^{-jk_x y} \\ \bar{E}_z e^{-jk_z y} \end{matrix}\right|_1 = \left|\begin{matrix} \dfrac{j\kappa^*}{\delta + \sqrt{\kappa^2 + \delta^2}} \\ 1 \end{matrix}\right| e^{-j(\bar{k} - \sqrt{\kappa^2 + \delta^2})y} \qquad \text{(A-7)}$$

$$\bar{k} \equiv \frac{1}{2}(k_x + k_z) \quad , \qquad \text{(A-8)}$$

while the second mode is

$$\left|\begin{matrix} E_x(y) \\ E_z(y) \end{matrix}\right|_2 = \left|\begin{matrix} \dfrac{j\kappa^*}{\delta - \sqrt{\kappa^2 + \delta^2}} \\ 1 \end{matrix}\right| e^{-j(\bar{k} + \sqrt{\kappa^2 + \delta^2})y} \quad . \qquad \text{(A-9}$$

Note: (1) When $\kappa >> \delta$, the eigenmodes become

$$\vec{E}_1 = \begin{vmatrix} E_x(y) \\ \\ E_z(y) \end{vmatrix} \approx \begin{vmatrix} j \\ \\ 1 \end{vmatrix} e^{-j\left[\frac{1}{2}(k_x+k_z)-\kappa\right]y} \tag{A-10}$$

$$\vec{E}_2 = \begin{vmatrix} E_x(y) \\ \\ E_z(y) \end{vmatrix} \approx \begin{vmatrix} -j \\ \\ 1 \end{vmatrix} e^{-j\left[\frac{1}{2}(k_x+k_z)+\kappa\right]y} \quad ; \tag{A-11}$$

i.e., the eigenmodes approach pure circular polarization.

(2) When $\kappa << \delta$ (this condition is important, since κ is a function of direction and can become zero), the modes approach:

$$\vec{E}_1 \quad \begin{vmatrix} 0 \\ 1 \end{vmatrix} e^{-jk_x y} \tag{A-12}$$

$$\vec{E}_2 \quad \begin{vmatrix} 1 \\ 0 \end{vmatrix} e^{-jk_z y} \quad ; \tag{A-13}$$

i.e., pure linear-polarized waves. The solution of Eq. A-6, subject to the boundary condition $E_z(0) = E_o$, $E_x(0) = 0$ is given by (A. Yariv, J. Quantum Electron. QE-9, 919, Sept. 1973),

$$E_x = E_o \frac{\kappa_{xz} e^{-j\delta y}}{(\kappa^2 + \delta^2)^{1/2}} \sin\left[(\kappa^2 + \delta^2)^{1/2} y\right] \quad , \tag{A-14a}$$

$$E_z = E_o e^{j\delta y} \left\{\cos\left[(\kappa^2 + \delta^2)^{1/2} y\right] - j \frac{\delta}{(\kappa^2 + \delta^2)^{1/2}} \sin\left[(\kappa^2 + \delta^2)^{1/2} y\right]\right\} , \tag{A-14b}$$

where $\kappa^2 = |\kappa_{xz}|^2 = |\kappa^*_{zx}|^2$.

Optical Activity + Electro-Optic Effect

If we also have an electro-optic effect or strain induced ε_{xz}, we must replace the matrix in A-5 with

$$\vec{P}_{NL} = \varepsilon_o \begin{vmatrix} 0 & ja + \varepsilon_{xz} \\ -ja + \varepsilon_{xz} & 0 \end{vmatrix} \quad . \tag{A-15}$$

This will cause the coupling coefficient to have the form $\kappa_{xz} = \kappa + j\Gamma$, and $\kappa_{zx} = -\kappa + j\Gamma$, since $\kappa_{zx} = -\kappa^*_{xz}$ (conservation of energy).

We thus replace $-k_o a/n$ by

$$-\frac{k_o a}{n} + j\,\frac{n^3 kr}{2}\,\mathcal{E}_{dc} \quad , \tag{A-16}$$

where r is the appropriate r_{ijk} tensor.

Equation A-14a becomes

$$E_x(y) = E_o\,\frac{(j\Gamma + \kappa)e^{-j\delta y}}{(\kappa^2 + \Gamma^2 + \delta^2)^{1/2}}\,\sin\left[(\kappa^2 + \Gamma^2 + \delta^2)^{1/2} y\right] \quad , \tag{A-17}$$

where $\kappa \rightarrow$ represents optical activity (or Faraday rotation), and

$\Gamma \rightarrow$ electro-optic effect (in which case it is proportional to $\mathcal{E}_{dc}$ or to strain in the case of the photoelastic effect).

APPENDIX B

DERIVATION OF EIGENMODES (A-7), (A-9)

We start with A-6 and write

$$\frac{dE_x}{dy} = \kappa E_z e^{-j2\delta y} \quad , \quad 2\delta = k_z - k_x$$

$$\frac{dE_z}{dy} = -\kappa^* E_x e^{j2\delta y} \quad , \quad \kappa = \frac{k_o a}{n} \quad . \tag{B-1}$$

We are looking for a linear combination of $E_x e^{-jk_x y}$ and $E_z e^{-jk_z y}$ which propagates with a constant complex ratio. We define a "vector"

$$\tilde{E} = \begin{vmatrix} E_z(y)\, e^{-jk_z y} \\ E_x(y)\, e^{-jk_x y} \end{vmatrix} \tag{B-2}$$

From B-1 above we have

$$\frac{d\tilde{E}}{dy} = \begin{vmatrix} -jk_z & -\kappa^* \\ \kappa & -jk_x \end{vmatrix} \tilde{E} \quad . \tag{B-3}$$

We look for a solution

$$\tilde{E}(y) = \tilde{E}(0)\, \exp(j\gamma y) = \begin{vmatrix} E_1 \\ E_2 \end{vmatrix} e^{j\gamma y} \quad . \tag{B-4}$$

This gives

$$-j(k_z + \gamma)E_1 - \kappa^* E_2 = 0$$

$$\kappa E_1 - j(k_x + \gamma)\, E_2 = 0 \qquad \text{(B-5)}$$

$$\gamma_{1,2} = -\frac{(k_x + k_z)}{2} \pm \frac{1}{2}\sqrt{(k_x - k_z)^2 + 4\kappa^2}$$

$$= -\bar{k} \pm s \qquad \text{(B-6)}$$

$$\bar{k} = \frac{1}{2}(k_x + k_z), \quad s = \sqrt{\kappa^2 + \delta^2}$$

$$\kappa^2 \equiv \kappa\kappa^* \qquad \delta \equiv \frac{1}{2}(k_z - k_x) \quad . \qquad \text{(B-7)}$$

The corresponding eigenvectors are obtained by putting B-6 in B-5:

$$\tilde{E}_1 = \begin{vmatrix} \dfrac{j\kappa^*}{\delta + \sqrt{\kappa^2 + \delta^2}} \\ 1 \end{vmatrix} e^{-j(\bar{k} - \sqrt{\kappa^2 + \delta^2})y}$$

$$\tilde{E}_2 = \begin{vmatrix} \dfrac{j\kappa^*}{\delta - \sqrt{\kappa^2 + \delta^2}} \\ 1 \end{vmatrix} e^{-j(\bar{k} + \sqrt{\kappa^2 + \delta^2})y} \quad . \qquad \text{(B-8)}$$

APPENDIX C

FARADAY ROTATION AND OPTICAL ACTIVITY

The two effects are similar with one basic difference. The gyrotropic polarization induced in Faraday rotation (FR) is described by

$$\vec{P}_{gyro} = j\epsilon_o \alpha \vec{B}x\vec{E} \quad , \tag{C-1}$$

where $\vec{B}$ is the magnetic field and $\vec{E}$ is the optical field. This can be described for propagation along $\vec{B}(\hat{z})$ by a tensor,

$$\vec{P}_{gyro} = \epsilon_o \begin{vmatrix} 0 & 0 & j\omega\epsilon_o B \\ 0 & 0 & 0 \\ -j\omega\epsilon_o B & 0 & 0 \end{vmatrix} \begin{vmatrix} E_x \\ E_y \\ E_z \end{vmatrix} \quad . \tag{C-2}$$

Optical activity (OA) is described by

$$\vec{P}_{opt.activ.} = j\omega\epsilon_o \vec{k}x\vec{E} \quad , \tag{C-3}$$

where $\vec{k}$ is the propagation vector. The basic difference between FR and OA is that $\vec{P}$ changes sign in OA when the direction of propagation changes sign, while in FR it does not. The ϵ tensor for optical rotation is

$$\vec{P}_{gyro} = \epsilon_o \begin{vmatrix} 0 & 0 & -j\omega k_y \\ 0 & 0 & 0 \\ j\omega k_y & 0 & 0 \end{vmatrix} \begin{vmatrix} E_x \\ E_y \\ E_z \end{vmatrix} \quad . \tag{C-4}$$

The matrix elements change sign when the $\vec{k}$ is reversed. This gives rise to the unwinding of the polarization "helix" in the reverse propagation.